CDDpress

www.nature.com/cdd

ARTICLE

Check for updates

Regulation of sclerostin by the SIRT1 stabilization pathway in osteocytes

Jung-Min Kim[1], Yeon-Suk Yang[1], Jun Xie[2,3,4], Oksun Lee[1], JiHea Kim[1], Jaehyoung Hong[5], Brigitte Boldyreff[6], Odile Filhol[7], Hyonho Chun[5], Matthew B. Greenblatt[8,9], Guangping Gao[2,3,4,10] and Jae-Hyuck Shim[1,2,10]✉

Osteocytes play a critical role in bone remodeling through the secretion of paracrine factors regulating the differentiation and activity of osteoblasts and osteoclasts. Sclerostin is a key osteocyte-derived factor that suppresses bone formation and promotes bone resorption, therefore regulators of sclerostin secretion are a likely source of new therapeutic strategies for treatment of skeletal disorders. Here, we demonstrate that protein kinase CK2 (casein kinase 2) controls sclerostin expression in osteocytes via the deubiquitinase ubiquitin-specific peptidase 4 (USP4)-mediated stabilization of Sirtuin1 (SIRT1). Deletion of CK2 regulatory subunit, *Csnk2b*, in osteocytes (*Csnk2b*^{Dmp1}) results in low bone mass due to elevated levels of sclerostin. This phenotype in *Csnk2b*^{Dmp1} mice was partly reversed when sclerostin expression was downregulated by a single intravenous injection with bone-targeting adeno-associated virus 9 (AAV9) carrying an artificial-microRNA that targets *Sost*. Mechanistically, CK2-induced phosphorylation of USP4 is important for stabilization of SIRT1 by suppressing ubiquitin-dependent proteasomal degradation. Upregulated expression of SIRT1 inhibits sclerostin transcription in osteocytes. Collectively, the CK2-USP4-SIRT1 pathway is crucial for the regulation of sclerostin expression in osteocytes to maintain bone homeostasis.

Cell Death & Differentiation (2022) 29:1625–1638; https://doi.org/10.1038/s41418-022-00952-x

INTRODUCTION

Bone is a dynamic tissue that remodels continuously throughout life and this remodeling activity is tightly controlled by the balance between bone-resorbing osteoclasts and bone-forming osteoblasts [1, 2]. Osteocytes, terminally differentiated osteoblast-lineage cells embedded in the mineralized bone matrix, also function as orchestrators of bone remodeling by transducing mechanical signals to bone through their dendritic projections and paracrine factors such as receptor activator of nuclear factor kappa-B ligand (RANKL), osteoprotegerin (OPG), dickkopf WNT signaling pathway inhibitor 1 (DKK1), and sclerostin, they in turn regulate the differentiation and activity of osteoblasts and osteoclasts [3–7].

Sclerostin (encoded by *Sost*), an antagonist of WNT signaling, interferes with the engagement of WNTs with the WNT receptor Frizzled by binding to co-receptors of WNTs, low-density lipoprotein receptor-related proteins 5 and 6 (LRP5/6), suppressing WNT-induced osteogenesis and bone formation [8]. In humans, a lack of sclerostin expression caused by loss-of-function mutations in the *SOST* gene locus causes sclerosteosis and Van Buchem disease (VBD), two rare skeletal disorders characterized by high bone mass [9–11]. As seen in human patients, *Sost*-deficient mice display a high bone mass phenotype with increased bone formation and bone strength [12, 13]. Conversely, overexpression of human *SOST* resulted in an osteopenic bone phenotype with low bone mineral density in mice [11]. While anti-sclerostin biologic drugs have been recently approved, cost and other limitations associated with biologic therapies largely limit the application of this therapy to a small subset of the potentially applicable patients. Identifying signaling pathways that regulate sclerostin expression may provide opportunities for the development of small molecules that suppress sclerostin expression that thereby avoids some of the limitations associated with current anti-sclerostin biologic agents.

In this study, we identified a novel pathway controlling sclerostin expression in osteocytes by which the deubiquitinase ubiquitin-specific peptidase 4 (USP4) stabilizes the histone deacetylase sirtuin 1 (SIRT1) via protein kinase CK2 (casein kinase 2)-mediated phosphorylation. SIRT1 functions as a positive regulator of bone mass and repressor of *Sost* expression by modifying H3K9 acetylation at its promoter [14–16]. Genetic deletion of *Sirt1* results in low bone mass due to decreased bone formation activity, while the SIRT1 activator SRT2104 preserves bone mass in aged mice [14, 16–18]. However, roles for the histone deacetylase SIRT1 and the DUB USP4 in osteocyte development remain unresolved. CK2 is a constitutively active serine/threonine kinase and composed of

[1]Department of Medicine, University of Massachusetts Medical School, Worcester, MA 01605, USA. [2]Horae Gene Therapy Center, University of Massachusetts Medical School, Worcester, MA 01605, USA. [3]Department of Microbiology and Physiological Systems, University of Massachusetts Medical School, Worcester, MA 01605, USA. [4]Viral Vector Core, University of Massachusetts Medical School, Worcester, MA 01605, USA. [5]Department of Mathematical Sciences, Korea Advanced Institute of Science and Technology, Daejeon 34141, Republic of Korea. [6]KinaseDetect ApS, 6340 Krusaa, Denmark. [7]Interdisciplinary Research Institute of Grenoble, IRIG-Biosanté, University Grenoble Alpes, CEA, UMR 1292, F-38000 Grenoble, France. [8]Department of Pathology and Laboratory Medicine, Weill Cornell Medical College, New York, NY 10065, USA. [9]Hospital for Special Surgery, New York, NY 10021, USA. [10]Li Weibo Institute for Rare Diseases Research, University of Massachusetts Medical School, Worcester, MA 01605, USA. ✉email: jaehyuck.shim@umassmed.edu
Edited by R. Damgaard

Received: 10 April 2021 Revised: 31 January 2022 Accepted: 2 February 2022
Published online: 15 February 2022

two catalytic α (*Csnk2a1*)- or α′ (*Csnk2a2*)-subunits and two regulatory β subunits (*Csnk2b*) [19–21]. The two catalytic subunits have high similarity in terms of their enzymatic functions whereas regulatory β-subunits bind the α-subunits and determine substrate specificity [22, 23]. Our previous study demonstrated that CK2 controls the commitment and differentiation of skeletal stem cells to osteoblasts via regulation of the master transcription factor RUNX2 [24]. Surprisingly, our current study suggests that CK2 function is specified according to cellular differentiation stage with different molecular mechanism. This study establishes a CK2-USP4-SIRT1 pathway controlling sclerostin expression as a fine-modulator of bone homeostasis.

RESULTS

CK2 negatively regulates osteocyte differentiation

Immunohistochemistry identified high expression of the regulatory subunit of CK2 CSNK2B in mature osteoblasts, bone-lining cells, and bone matrix-embedded osteocytes in mice (Fig. 1a). This is consistent with immunofluorescence analysis showing the expression of CSNK2B in osteocalcin$^+$ mature osteoblasts and sclerostin$^+$ osteocytes in femoral bone (Supplementary Fig. 1). In addition to CSNK2B expression in skeletal stem cells/progenitors residing in the perichondrium and growth plate from our previous study, this result suggests that CK2 might have different function in late stage of osteogenesis [24]. In particular, CSNK2B expression was primarily located in endosteal osteoblasts and osteocytes. This CSNK2B expression was detected in osteoblasts and osteocytes with dentin matrix protein 1 (*Dmp1*) promoter-driven expression of GFP in the femurs of *Dmp1;Rosa26*$^{mT/mG}$ mice (Supplementary Fig. 2), and therefore *Csnk2b* was conditionally deleted in endosteal osteoblasts and osteocytes by crossing *Csnk2b*-floxed allele (*Csnk2b*$^{fl/fl}$) with a Dmp1-Cre allele (*Csnk2b*^{Dmp1}) [25, 26]. The deletion efficiency of *Csnk2b* was confirmed by mRNA levels in the tibia of *Csnk2b*^{Dmp1} mice (Fig. 1b). In comparison with wildtype littermate control mice (*Csnk2b*$^{fl/fl}$), *Csnk2b*^{Dmp1} mice display increased numbers of osteocytes embedded in cortical and trabecular bones (Fig. 1c and Supplementary Fig. 3a). Additionally, expression of osteocyte differentiation genes, including *Dmp1*, metalloendopeptidase homolog PEX (*Phex*), E11/podoplanin (*Pdpn*), sclerostin (*Sost*), tumor necrosis factor (ligand) superfamily, member 11 (*Tnfsf11*, RANKL), and osteoprotegerin (*Tnfrsf11b*, OPG) were markedly increased in the tibia of *Csnk2b*^{Dmp1} mice (Fig. 1d and Supplementary Fig. 4), suggesting that deletion of *Csnk2b* in endosteal osteoblasts and osteocytes may enhance overall osteocyte differentiation. To test this hypothesis in vitro, DMP1-expressing Ocy454 osteocyte cell line generated from the DMP1-GFP transgenic mice was utilized [27]. All of three CK2 subunits, including *Csnk2a1*, *Csnk2a2*, and *Csnk2b*, were expressed in this cell line and their expression was increased in *Sost*-expressing mature osteocytes (Fig. 1e). As seen in *Csnk2b*^{Dmp1} mice (Fig. 1d), shRNA-mediated knockdown of *Csnk2b* results in a significant increase in the expression of both early and late osteocyte differentiation genes (Fig. 1f). Similarly, treatment with a CK2 inhibitor (Casein Kinase II inhibitor IV) upregulated expression of osteocyte differentiation genes (Supplementary Fig. 5). To further define CK2 function in osteocyte development, we performed morphologic analysis of osteocyte dendritic process. In vitro culture of osteocytes isolated from *Csnk2b*^{Dmp1} mice demonstrated enhanced dendrite numbers (Fig. 1g), while dendrite morphogenesis and connectivity were also increased in matrix-embedded *Csnk2b*^{Dmp1} osteocytes relative to *Csnk2b*$^{fl/fl}$ osteocytes (Fig. 1h). These results demonstrate that CK2 functions as a negative regulator of osteocyte differentiation.

Since GFP proteins are also detected in mature osteoblasts residing on the surface of *Dmp1;Rosa26*$^{mT/mG}$ femurs (Supplementary Fig. 2), we examined the function of CK2 specifically during the late stage of osteoblast differentiation (Supplementary Fig. 6). Primary calvarial osteoblasts (COBs) obtained from *Csnk2b*$^{fl/fl}$ neonates were transduced with lentivirus carrying CRE recombinase (*ΔCsnk2b*) or a vector control (WT) starting six days after initiating osteogenic differentiation. These mature osteoblasts were then further differentiated up to eighteen days, demonstrating an at most modest reduction of mineralization activity and osteogenic gene expression in *Csnk2b*-deficient osteoblasts. Taken together, CK2 deficiency upregulates osteocyte development while its effect is minimal on the late stage differentiation of mature osteoblasts.

Csnk2b^{Dmp1} mice display severe osteopenia

Despite increased numbers of osteocytes embedded in the bone matrix, *Csnk2b*^{Dmp1} mice displayed low bone mass in long bones as trabecular bone mass and cortical bone thickness were both markedly reduced (Fig. 2a, b and Supplementary Fig. 7). This phenotype is similar in both sexes of *Csnk2b*^{Dmp1} mice (Supplementary Fig. 7). Biomechanical testing showed that the strength and stiffness of femurs were considerably decreased in *Csnk2b*^{Dmp1} mice compared to *Csnk2b*$^{fl/fl}$ mice (Fig. 2c). Dynamic histomorphometry revealed a reduction of bone formation rate (BFR) in the femur of *Csnk2b*^{Dmp1} mice while mineralization apposition rate (MAR) was relatively comparable between *Csnk2b*$^{fl/fl}$ and *Csnk2b*^{Dmp1} femurs (Fig. 2d, e). Remarkably, numbers of tartrate-resistant acid phosphatase (TRAP)- or cathepsin K-expressing osteoclasts on the bone surface, serum levels of the pro-osteoclastogenic factor RANKL, and the bone resorption marker C-terminal telopeptide type I collagen (CTx-I) were substantially increased in *Csnk2b*^{Dmp1} mice (Fig. 2f, g and Supplementary Fig. 3b). These results suggest that *Csnk2b* deficiency in osteoblasts/osteocytes results in osteopenia in *Csnk2b*^{Dmp1} mice by suppressing osteoblast-mediated bone formation and promoting osteoclast-mediated bone resorption simultaneously.

CSNK2B deficiency upregulates sclerostin expression in osteocytes

Osteocytes have been reported to control osteoblast and osteoclast differentiation via paracrine factors, including RANKL, OPG, and sclerostin [7, 28, 29]. To define the effect of *Csnk2b*-deficient osteocytes-derived secretory factors on osteoblast and osteoclast, wildtype bone marrow-derived stromal cells (BMSCs) were treated with conditioned medium (CM) harvested from *Csnk2b*-sufficient (*shScr*) or -deficient (*shCsnk2b*) osteocytes. Alkaline phosphatase activity (Fig. 3a) and expression of osteogenic genes, including bone sialoprotein 2 (*Ibsp*) and osteocalcin (*Bglap*) (Fig. 3b) were markedly reduced in the presence of the CM of *shCsnk2b*-expressing osteocytes compared to the CM of *shScr*-expressing osteocytes, suggesting that *shCsnk2b*-expressing osteocytes secret osteogenic inhibitor(s). On the other hand, when cultured with wildtype bone marrow-derived monocytes (BMM) under osteoclastogenic conditions, the CM of *shCsnk2b*-expressing osteocytes substantially increased TRAP staining and activity and expression of osteoclast differentiation genes, including cathepsin K (*Ctsk*), nuclear factor of activated T cells 1 (*Nfatc1*), and tartrate-resistant acid phosphatase type 5 (*Acp5*) (Fig. 3c–e), suggesting that *shCsnk2b*-expressing osteocytes also secret pro-osteoclastogenic factor(s). Notably, these paracrine effects of *Csnk2b* deficiency on the differentiation of osteoblasts and osteoclasts are intrinsic to osteocytes. Unlike CM of *shCsnk2b*-expressing osteocytes, at most modest effect of CM of *Csnk2b*-deficient osteoblasts on osteogenesis of wildtype BMSCs (Supplementary Fig. 8a, b) or osteoclastogenesis of wildtype BMMs (Supplementary Fig. 8c–e). The observation that the paracrine effects of *Csnk2b*-deficient osteoblasts on osteoblast or osteoclast differentiation are milder than those of *Csnk2b*-deficient osteocytes are most consistent with *Csnk2b* deficiency in osteocytes being the major driver of low bone mass in *Csnk2b*^{Dmp1} mice.

Next, we sought to identify the anti-osteogenic and pro-osteoclastogenic factors secreted from *Csnk2b*-deficient osteocytes using transcriptome analysis. Total mRNAs were extracted

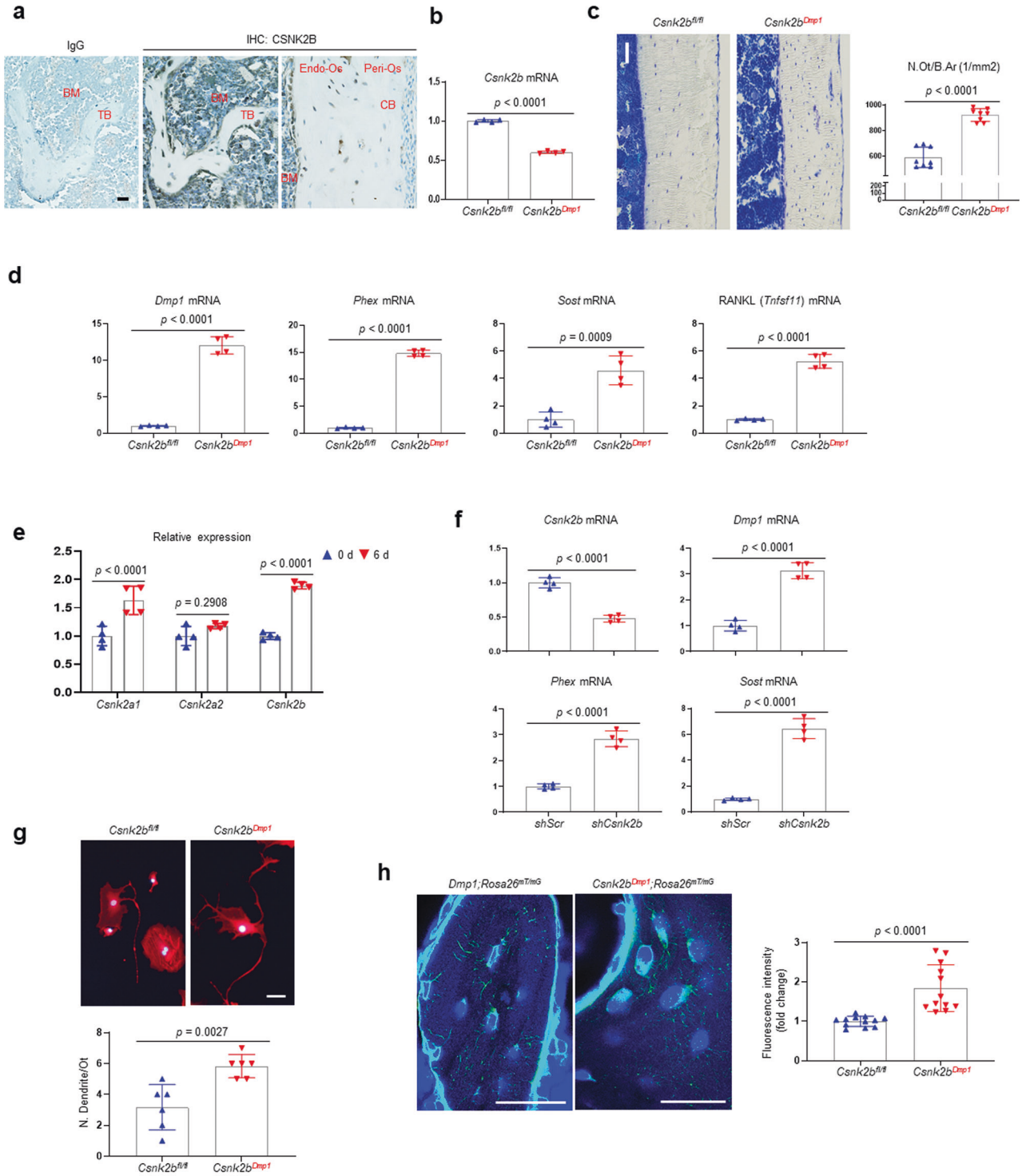

from *shScr*- or *shCsnk2b*-expressing osteocytes, subjected to bulk RNA sequencing, and secreted proteins with differential expression in these cells were selected (Fig. 3f). Transcriptome analysis of *Csnk2b*-deficient osteocytes confirmed a knockdown efficiency of *Csnk2b* and upregulation of osteocyte differentiation genes including *Phex* and *Sost*. Among top thirty genes with the highest or lowest differential expression (Fig. 3f), sclerostin was selected as an osteocyte-derived secretory protein that has both anti-osteogenic and pro-osteoclastogenic potentials. Consistent with elevated mRNA levels of *Sost* in *Csnk2b*-deficient osteocytes and $Csnk2b^{Dmp1}$ femurs (Fig. 1d, f), protein levels of sclerostin were markedly increased in *Csnk2b*-deficient osteocytes and $Csnk2b^{Dmp1}$ tibias (Fig. 3g). Additionally, numbers of sclerostin-expressing osteocytes in the cortical bone of $Csnk2b^{Dmp1}$ mice are increased (Fig. 3h). Since sclerostin functions as a negative regulator of WNT/β-catenin signaling, upregulation of sclerostin by *Csnk2b* deficiency could inhibit β-catenin transcription activity. Tibias from $Csnk2b^{Dmp1}$ mice showed reduced expression of a β-catenin target gene *Axin2* compared to $Csnk2b^{fl/fl}$ tibia (Fig. 3i). Additionally, treatment of wildtype osteoblasts with the CM of

Fig. 1 CK2 signaling negatively regulates osteocyte differentiation. **a** Immunohistochemistry (IHC) for CSNK2B in 8-week-old mouse femurs. Left, IgG control; middle, IHC for CSNK2B in the trabecular bone; right, IHC for CSNK2B in the cortical bone. BM bone marrow, TB trabecular bone, CB cortical bone, Endo-Os endosteum, Peri-Os periosteum. Scale bar, 20 μm. **b** *Csnk2b* mRNA levels in the tibia of 8-week-old *Csnk2b*$^{fl/fl}$ and *Csnk2b*^{Dmp1} mice were assessed by RT-PCR and normalized to *Rplp0* ($n = 4$/group). **c** Toluidine blue staining of 8-week-old *Csnk2b*$^{fl/fl}$ and *Csnk2b*^{Dmp1} cortical bones (left) and quantification of bone matrix-embedded osteocytes (right). Scale bar, 50 μm. **d** mRNA levels of osteocyte differentiation genes in 8-week-old *Csnk2b*$^{fl/fl}$ and *Csnk2b*^{Dmp1} tibias. **e** mRNA levels of CK2 subunits in Ocy454 osteocyte cell line at day 0 and day 6 post-differentiation were assessed by RT-PCR and normalized to *Rplp0* ($n = 4$/group). **f** Ocy454 cells infected with lentiviruses expressing *shScr* (control) or *shCsnk2b* (*Csnk2b*-knockdown) were cultured under differentiation condition for six days and mRNA levels of osteocyte differentiation genes were measured by RT-PCR. **g** Osteocyte-enriched fraction was harvested from 8-week-old *Csnk2b*$^{fl/fl}$ and *Csnk2b*^{Dmp1} femurs and tibias and cells in the fraction were cultured for 28 days. After phalloidin (red) staining, osteocyte morphology was assessed using fluorescence microscopy (top). Quantification of dendrite numbers per osteocyte was also displayed (bottom). Scale bar, 50 μm. **h** Femoral sections of 8-week-old *Dmp1;Rosa26*$^{mT/mG}$ and *Csnk2b*^{Dmp1}*;Rosa26*$^{mT/mG}$ mice were stained with DAPI and morphology of GFP-expressing DMP1^{+} osteocytes was analyzed by fluorescence microscopy (left). To show osteocyte network formation, fluorescence intensity of GFP-expressing dendrites was determined by ImageJ software (right). Scale bar, 250 μm. Data are representative of three independent experiments. A two-tailed unpaired Student's *t*-test for comparing two groups (**b**–**h**; error bars, SD of biological replicates).

Csnk2b-deficient osteocytes decreased β-catenin-responsive luciferase activity (Fig. 3j) and *Axin2* expression (Fig. 3k), suggesting that sclerostin secreted from *Csnk2b*-deficient osteocytes inhibits WNT/β-catenin signaling. Previous studies have demonstrated that sclerostin upregulates the ratio of RANKL to the RANKL-inhibitor OPG in osteocytes, promoting osteoclast differentiation [30–33]. Intriguingly, *Csnk2b*-deficient osteocytes also showed increased RANKL (*Tnfsf11*) and decreased OPG (*Tnfrsf11b*) expression, suggesting that elevated levels of sclerostin in *Csnk2b*-deficient osteocytes may increase the RANKL/OPG ratio and enhance osteoclast differentiation (Supplementary Fig. 9). To examine the contribution of the increased RANKL/OPG ratio to this ability of *Csnk2b*-deficient osteocytes to promote osteoclast differentiation, the RANKL-inhibitor OPG-Fc was added to cultures of wildtype BMMs and these BMMs underwent osteoclast differentiation in the presence of CM from *Csnk2b*-deficient osteocytes, demonstrating that OPG-Fc treatment reversed the enhanced osteoclast differentiation driven by *Csnk2b*-deficient osteocytes CM (Supplementary Fig. 10a–c). As expected, OPG-Fc treatment did not impact the suppression of osteoblast differentiation by CM from *Csnk2b*-deficient osteocytes (Supplementary Fig. 10d, e). Thus, an increased RANKL/OPG ratio by sclerostin in *Csnk2b*-deficient osteocytes is a major contributor to their ability to drive enhanced osteoclast differentiation. Taken together, these results suggest that sclerostin secreted from *Csnk2b*-deficient osteocytes suppresses osteoblast differentiation by inhibiting WNT/β-catenin signaling and promotes osteoclast differentiation by upregulating the RANKL/OPG ratio, which results in osteopenia of *Csnk2b*^{Dmp1} mice.

AAV-mediated silencing of sclerostin reverses osteopenia in *Csnk2b*^{Dmp1} mice

To test this hypothesis, we examined whether downregulation of sclerostin expression can reverse the existing bone phenotype of *Csnk2b*^{Dmp1} mice. Our previous study demonstrated that recombinant adeno-associated virus serotype 9 (rAAV9) is highly effective for transduction of osteoblast-lineage cells, including endosteal osteoblasts and osteocytes [34]. We therefore constructed amiR cassettes containing two mouse *Sost* targeting sequences (*amiR-Sost1*, *amiR-Sost2*) or a control (*amiR-Ctrl*). In this design, the amiR is inserted intronically between the *CB* promoter and the *Egfp* reporter gene (Fig. 4a), which allows for visual tracking of positively transduced tissues (Fig. 4b). As expected, GFP proteins were highly expressed in endosteal osteoblasts and osteocytes embedded in the cortical bone at 2 months after intravenous (i.v.) injection of rAAV9.egfp (Fig. 4c). When i.v. injected into 12-week-old wildtype mice, compared to *amiR-Ctrl*-treated mice, treatment with rAAV9 carrying *amiR-Sost1* or *amiR-Sost2* resulted in ~25 or ~55% decrease of *Sost* mRNA levels in the tibia, respectively (Fig. 4d). This is corresponding to an increase in trabecular bone mass of AAV-treated femurs, as shown by greater trabecular bone volume per tissue volume (Tb. BV/TV), number (Tb. N), and thickness (Tb. Th) (Fig. 4e, f). Since a bone-specific tropism of AAV9 capsid was improved by grafting the bone-targeting peptide motif $(AspSerSer)_6$ onto the AAV9-VP2 capsid protein (AAV9.DSS-Nter) [34, 35], *amiR-Sost2* that shows a higher knockdown efficiency than *amiR-Sost1* (Fig. 4d) was packaged into the AAV9.DSS-Nter capsid (rAAV9.DSS-Nter-*amiR-Sost2*).

To examine the ability of bone-targeting AAV-mediated silencing of *Sost* to reverse osteopenia in *Csnk2b*^{Dmp1} mice, 8-week-old *Csnk2b*$^{fl/fl}$ and *Csnk2b*^{Dmp1} mice were treated with a single i.v. injection of rAAV9.DSS-Nter carrying *amiR-Ctrl* or *amiR-Sost2* and 2 months later, skeletal phenotype was assessed by microCT analysis. Deletion of *Csnk2b* and knockdown efficiency of *Sost* expression in tibia were validated by RT-PCR analysis (Fig. 4g). Expression of a β-catenin target gene *Axin2* was markedly upregulated in *amiR-Sost2*-expressing *Csnk2b*^{Dmp1} tibia relative to *amiR-Ctrl*-expressing *Csnk2b*^{Dmp1} tibia, demonstrating that bone-targeting AAV-mediated silencing of *Sost* expression enhances WNT signaling in *Csnk2b*^{Dmp1} mice (Fig. 4h). This is accompanied with a significant reduction of RANKL/OPG ratio in *Csnk2b*^{Dmp1} tibia following the treatment with AAV9.DSS-Nter. *amiR-Sost2* (Fig. 4i), suggesting that *Csnk2b* deficiency in osteocytes upregulates the RANKL/OPG ratio via sclerostin. Accordingly, while *amiR-Ctrl*-expressing *Csnk2b*^{Dmp1} mice showed a significant reduction in trabecular bone mass relative to *Csnk2b*$^{fl/fl}$ mice, low bone mass was partially reversed in the femurs of *Csnk2b*^{Dmp1} mice treated with rAAV9.DSS-Nter-*amiR-Sost2*, as shown by greater trabecular BV/TV, number, and thickness (Fig. 4j, k). Thus, these results suggest that elevated levels of sclerostin in *Csnk2b*-deficient osteocytes are at least partially responsible for the osteopenia seen in *Csnk2b*^{Dmp1} mice, which can be reversed by bone-targeting AAV9-mediated silencing of *Sost*.

CK2 stabilizes SIRT1 via the deubiquitinating enzyme USP4

Among osteocytic proteins regulating sclerostin expression, the class III histone deacetylase (HDAC) sirtuin 1 (SIRT1) has been identified as a potential CK2 substrate in human tissues [36–38]. To test this possibility in osteocytes, a pull-down assay was performed in the Ocy454 cell line, demonstrating that SIRT1 interacts with CSNK2B in osteocytes (Fig. 5a). Intriguingly, protein levels of SIRT1 were markedly decreased in *Csnk2b*-deficient osteocytes without any alteration in *Sirt1* mRNA levels, and this effect was reversed by treatment with the proteasomal inhibitor MG132 (Fig. 5b, c). This was accompanied with increased ubiquitination levels of SIRT1 in *Csnk2b*-deficient osteocytes when treated with MG132 (Fig. 5d). Similarly, inhibition of CK2 kinase activity enhanced SIRT1 ubiquitination (Supplementary Fig. 11a). These results suggest that CK2 kinase activity is important for stabilization of SIRT1 protein in osteocytes by suppressing SIRT1 ubiquitin-dependent proteasomal degradation. Similar to *Csnk2b*-deficient osteocytes, *Sirt1* deficiency in osteocytes enhanced

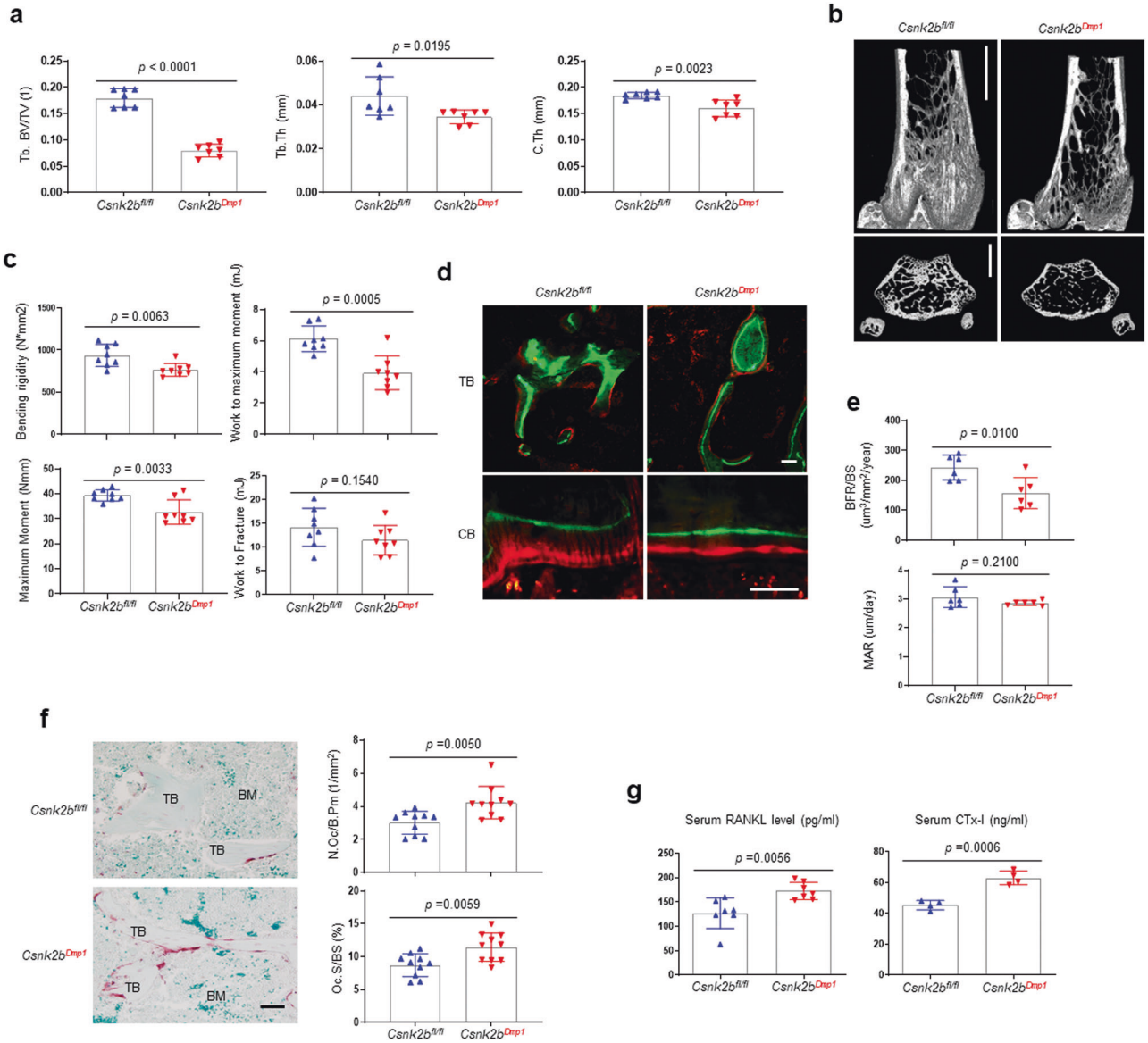

Fig. 2 ***Csnk2b^Dmp1* mice display severe osteopenia.** **a**, **b** MicroCT analysis showing a decrease of femoral bone mass in eight-week-old *Csnk2b^fl/fl* and *Csnk2b^Dmp1* male mice. Quantification (**a**) and 3D-reconstruction (**b**) are displayed. Trabecular bone volume/total volume (Tb. BV/TV), trabecular thickness (Tb.Th), and cortical thickness (C.Th) were measured. Scale bar, 1 mm (**b**). **c** Biomechanical properties of 8-week-old *Csnk2b^fl/fl* and *Csnk2b^Dmp1* femurs, including bending rigidity, maximum moment, work to maximum moment, and work to fracture were quantified using three-point bending test. **d**, **e** Dynamic histomorphometric analysis of eight-week-old *Csnk2b^fl/fl* and *Csnk2b^Dmp1* femurs. Representative images of calcein/alizarin red labeling of trabecular (**d**, top) and cortical bone (**d**, bottom) and relative histomorphometric quantification of BFR/BS and MAR (**e**). Scale bar, 50 μm (**d**). TB trabecular bone, CB cortical bone, BFR/BS bone formation rate per bone surface, MAR mineral apposition rate. **f** TRAP-stained longitudinal sections of eight-week-old *Csnk2b^fl/fl* and *Csnk2b^Dmp1* femurs. Representative images (left) and relative quantification (right) are shown. Scale bar, 50 μm (**g**, left). BM bone marrow, TB trabecular bone, N.Oc/B.pm osteoclast number per bone perimeter, Oc.S/BS osteoclast surface per bone surface. **g** Serum levels of receptor activator of nuclear factor kappa-B ligand (RANKL) and cross-linked C-telopeptide of type 1 collagen (CTx-I) in eight-week-old *Csnk2b^fl/fl* and *Csnk2b^Dmp1* male mice were measured by ELISA. Data are representative of three independent experiments (**b**, **d**, **f** [left]) or are pooled from two experiments (**a**, **c**, **e**, **f** [right], **g**). A two-tailed unpaired Student's *t*-test for comparing two groups (**a**, **c**, **e**–**g**; error bars, SD of biological replicates).

expression of osteocyte differentiation genes, including *Sost*, *Dmp1*, and *Phex*, suggesting that SIRT1 may also act as a negative regulator of osteocyte differentiation (Fig. 5e). Thus, CK2-mediated stabilization of SIRT1 is likely to be important for suppressing sclerostin expression in osteocytes.

To achieve further mechanistic insight into CK2-mediated stabilization of SIRT1, we hypothesized that SIRT1 stabilization may require the activity of specific deubiquitinating enzymes (DUBs). Thus, to screen SIRT1-regulating DUBs, we co-transfected HEK293 cells with a panel of candidate DUBs and assessed their interactions and ubiquitination of SIRT1 (Supplementary Fig. 12). Among eighteen DUBs tested, including the twelve ubiquitin-specific peptidases (USPs), four ovarian tumor proteases (OTUDs), and two Josephin domain-containing proteins (JOSDs), we identified USP4 and USP22 as SIRT1-interacting DUBs that inhibited the ubiquitination of SIRT1 (Fig. 6a, b and Supplementary Fig. 13a). USP22 has been reported to deubiquitinate and stabilize SIRT1 in non-bone cells [39], whereas USP4 was newly identified in this study. In vitro deubiquitination assays demonstrate that as with USP22, enforced expression of USP4 suppressed SIRT1

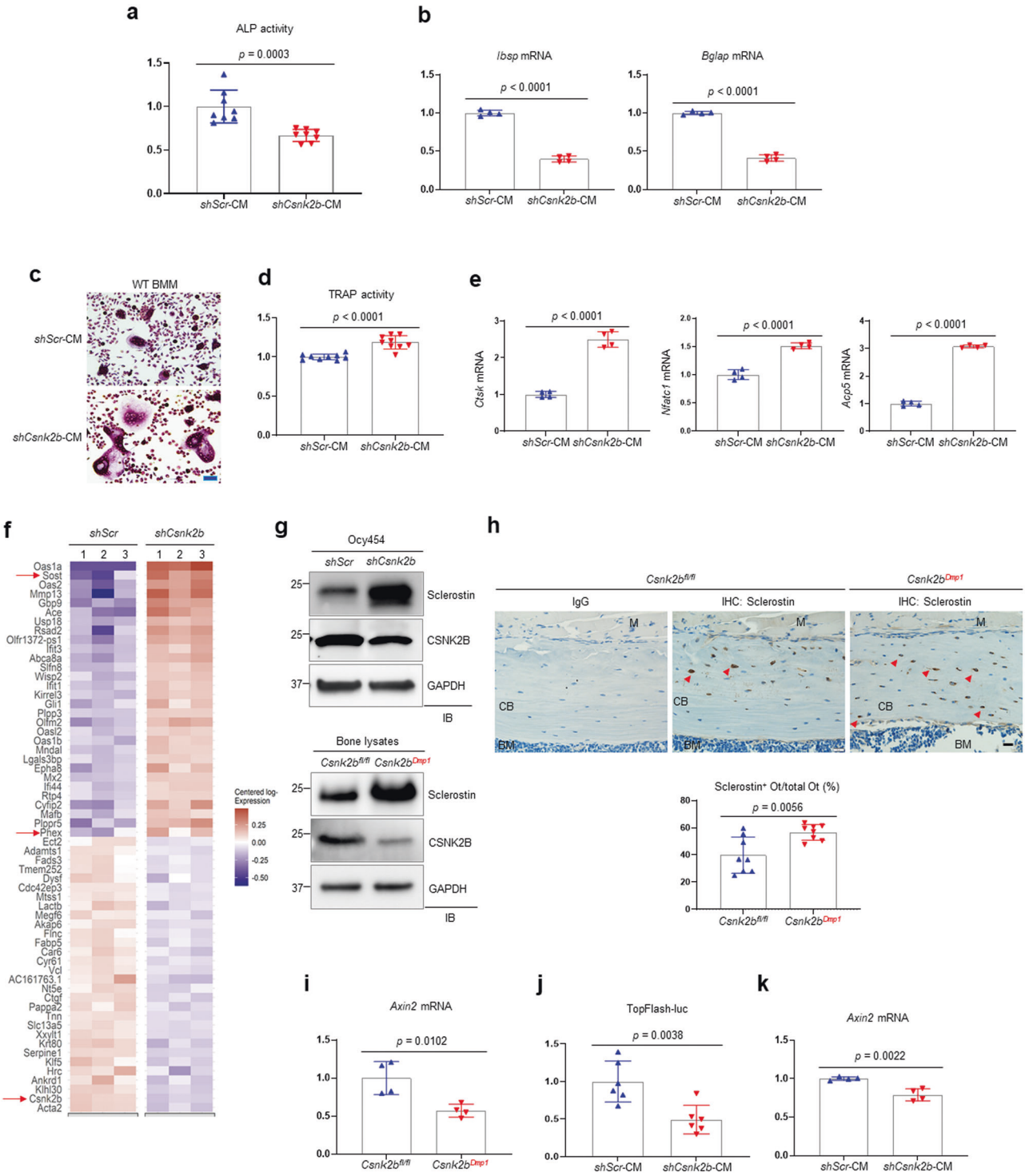

ubiquitination (Fig. 6c and Supplementary Fig. 13b). However, ubiquitination levels of SIRT1 in the osteocyte line were substantially upregulated by knockdown of USP4, not USP22 (Fig. 6d). Similarly, inhibition of USP4 DUB activity enhanced SIRT1 ubiquitination (Supplementary Fig. 11b), suggesting that USP4 might stabilize SIRT1 in osteocytes by deubiquitinating SIRT1.

Given that CK2 functions as a SIRT1 kinase in human cells [36, 37], we investigated the mechanism by which CK2 mediates SIRT1 stabilization by the DUB USP4 (Fig. 6e, f). The interaction between SIRT1 and USP4 was not affected by inhibition of CK2 kinase activity (Fig. 6e), suggesting that CK2-induced phosphorylation is dispensable for the interaction between SIRT1 and USP4. However, USP4-mediated deubiquitination of SIRT1 was markedly reduced in the presence of the CK2 inhibitor (Fig. 6f and Supplementary Fig. 13c). Previous studies have reported that USP4 contains several consensus sequences for CK2-mediated phosphorylation (S/T-X-X-D/E) [40] and that its DUB activity can be regulated by posttranslational modifications, such as phosphorylation [41, 42]. Indeed, phosphorylation levels of USP4 were markedly reduced in *Csnk2b*-deficient osteocytes, demonstrating

Fig. 3 CSNK2B deficiency in osteocytes upregulates sclerostin expression. a, **b** WT BMSCs were cultured under osteogenic conditions in the presence of the conditioned medium (CM) harvested from *shScr*- or *shCsnk2b*-expressing Ocy454 cells, and six days later, ALP activity (**a**) and osteogenic gene expression (**b**) were analyzed. **c**–**e** The CM harvested from *shScr*- or *shCsnk2b*-expressing Ocy454 cells six days after differentiation was added to mouse BMMs and cultured under osteoclast differentiation condition for 12 days. Osteoclast differentiation was assessed by TRAP staining (**c**), TRAP activity (**d**), and osteoclast gene expression (**e**). Scale bar, 50 μm (**c**). **f** Heat map showing differential gene expression in *shScr*- and *shCsnk2b*-expressing Ocy454 cells. Top 30 genes with upregulated or downregulated expression are presented (triplicates/group). The log10 expression (read count) was centered across samples. Red and purple denote upregulation and downregulation, respectively. (absolute log2 fold change >1.2 in *Csnk2b*-deficient osteocytes as compared to control). Arrows indicate upregulated expression of *Sost* and *Phex* and knockdown of *Csnk2b* expression in *Csnk2b*-deficient osteocytes as compared to control. **g** Immunoblot analysis showing protein levels of sclerostin and CSNK2B in *shScr*- and *shCsnk2b*-expressing Ocy454 cells six days after osteocyte differentiation (top) and in $Csnk2b^{fl/fl}$ and $Csnk2b^{Dmp1}$ tibias (bottom). **h** Immunohistochemistry for sclerostin in the cortical bone of eight-week-old $Csnk2b^{fl/fl}$ and $Csnk2b^{Dmp1}$ femurs (top). Numbers of sclerostin-expressing osteocytes per total osteocytes were quantitated (bottom). IgG was used for negative staining. Scale bar, 20 μm (top). M muscle, BM bone marrow, CB cortical bone. Arrows indicate sclerostin-expressing osteocytes. **i** *Axin2* mRNA levels in 8-week-old $Csnk2b^{fl/fl}$ and $Csnk2b^{Dmp1}$ tibias were assessed by RT-PCR and normalized to *Rplp0* ($n = 4$/group). **j** C3H10T1/2 cells were transfected with the TopFlash reporter gene along with *Renilla* and incubated with the CM obtained from *shScr*- or *shCsnk2b*-expressing Ocy454 cells. After 48 h, luciferase activity was measured and normalized to *Renilla*. **k** WT BMSCs were treated with CM of *shScr*- or *shCsnk2b*-expressing Ocy454 cells under osteogenic differentiation condition, *Axin2* mRNA levels were assessed at day 6 by RT-PCR ($n = 4$/group). Data are representative of three (**a**–**e**, **g**–**k**). A two-tailed unpaired Student's *t*-test for comparing two groups (**a**, **b**, **d**, **e**, **h**–**k**; error bars, SD of biological replicates).

that CK2 phosphorylates USP4 in osteocytes (Fig. 6g). Thus, CK2-induced phosphorylation of USP4 in osteocytes mediates USP4-mediated deubiquitination of SIRT1, not the interaction between USP4 and SIRT1. Similar to *Csnk2b*-deficient osteocytes, *Usp4*-deficient osteocytes showed decreased protein levels of SIRT1 along with increased protein levels of sclerostin, which was reversed by the treatment with the proteasomal inhibitor MG132 (Fig. 6h). Notably, elevated levels of *Sirt1* mRNA in *Usp4*-deficient osteocytes may result from a compensatory mechanism as SIRT1 protein levels are decreased by *Usp4* deficiency (Fig. 6i). Thus, USP4 likely upregulates SIRT1 expression at the posttranslational, not transcriptional levels. Finally, *Usp4* deficiency enhanced expression of characteristic osteocyte genes, as shown by the elevated mRNA levels of *Dmp1* and *Sost* (Fig. 6i), suggesting a negative role of USP4 in osteocyte development by controlling SIRT1 stability. Taken together, these results demonstrate that CK2-induced phosphorylation of USP4 is important for SIRT1 stabilization in osteocytes via USP4-mediated deubiquitination, ultimately suppressing *Sost* transcription.

DISCUSSION

Our data revealed that CK2 controls bone remodeling via an unexpected regulatory mechanism of sclerostin expression. Impaired CK2 function in osteocytes results in an increase in sclerostin production, leading to low bone mass. CK2 phosphorylates the DUB USP4, and subsequently phosphorylated USP4 removes ubiquitin from SIRT1, preventing its proteasome-dependent degradation. Alternatively, given previous studies demonstrating that CK2-mediated phosphorylation controls the histone deacetylase activity of SIRT1 and its substrate-binding affinity in non-bone cells [36, 43, 44], CK2 might also induce phosphorylation of SIRT1 in osteocytes, contributing to SIRT1 stabilization. Upregulation of SIRT1 suppresses sclerostin transcription by deacetylating histone 3 at lysine 9 at the sclerostin promoter [14]. Reduced levels of sclerostin simultaneously enhance osteoblast-mediated bone formation by upregulating WNT signaling and decrease osteoclast-mediated bone resorption by downregulating the RANKL/OPG ratio. Thus, CK2/USP4-mediated stabilization of SIRT1 in osteocytes is crucial for the maintenance of bone homeostasis via controlling sclerostin expression (Fig. 7). Further studies will be necessary to examine CK2-induced phosphorylation of SIRT1 in osteocytes and specifically whether the histone deacetylase activity of phosphorylated SIRT1 is altered in osteocytes, as these areas were not addressed by the present data. Additionally, the role of USP4 in osteocyte development is also not addressed by the present data will require further study.

Previous studies have demonstrated that SIRT1 plays a role in bone remodeling by promoting bone formation and inhibiting bone resorption and that SIRT1-dependent suppression of sclerostin expression contributes to increased bone mass mediated by SIRT1 activation [14, 16, 45]. SIRT1 also exerts its effect on bone metabolism through direct actions on osteoblasts and osteoclasts and SIRT1 function is likely to rely on cellular context according to age and sex [45–47]. However, the role for SIRT1 in osteocytes remains largely unknown. A previous study demonstrated the importance of the USP4 in early osteogenic differentiation of mesenchymal progenitors in vitro in that USP4 inhibits Wnt/β-catenin signaling by blocking proteasomal degradation of Disheveled (Dvl) [48]. However, its functions in osteoblast precursors and bone formation are controversial and in vivo skeletal phenotype according to differentiation stage was not fully studied [48–50]. Moreover, there are no studies showing its function in osteocyte biology. In this study, we identify roles for the CK2-USP4-SIRT1 signaling axis in both a completely different cell type (osteocytes) and with respect to completely different biologic and biochemical function (regulation of sclerostin expression). Further study will be needed to investigate in vivo roles for SIRT1 and USP4 using mice with conditional deletion of SIRT1 or USP4 in osteocytes ($Sirt1^{Dmp1}$, $Usp4^{Dmp1}$ mice). $Csnk2b^{Dmp1}$ mice have an important limitation in their ability to differentiate the contribution of CK2 deficiency in mature osteoblasts versus osteocytes as DMP1-Cre deletes *Csnk2b* in both cell types. Thus, it cannot be excluded that the function of CK2 in mature osteoblasts also contributes to the phenotypes observed.

It is important to emphasize that, while our AAV-mediated gene silencing studies suggest that sclerostin is a physiologic relevant target of the CK2/USP4/SIRT1 pathway in vitro and in vivo, they do not exclude that this pathway has other molecular targets in osteocytes and mature osteoblasts. CK2 signaling plays a role in cellular homeostasis, including regulation of cell cycle progression, proliferation, and differentiation [21, 40]. Notably, while CK2 deletion at early cell proliferation stage impaired the differentiation of skeletal stem cells to osteoblast progenitors, the differentiation of endosteal bone lining cells to osteocytes was enhanced when CK2 signaling was inhibited at post-mitotic cell stage [24] (Fig. 1). Additionally, mice lacking CK2 in osteoclasts did not show any skeletal phenotypes, demonstrating that CK2 is dispensable for osteoclast function [24]. These results suggest that CK2 functions may be dependent on differentiation stage and cellular context. Moreover, although elevated levels of sclerostin in *Csnk2b*-deficient osteocytes might be responsible for low bone mass in $Csnk2b^{Dmp1}$ mice, this phenotype was partially reversed by bone-targeting AAV-mediated silencing of sclerostin expression (Fig. 4). This partial rescue may be improved by further

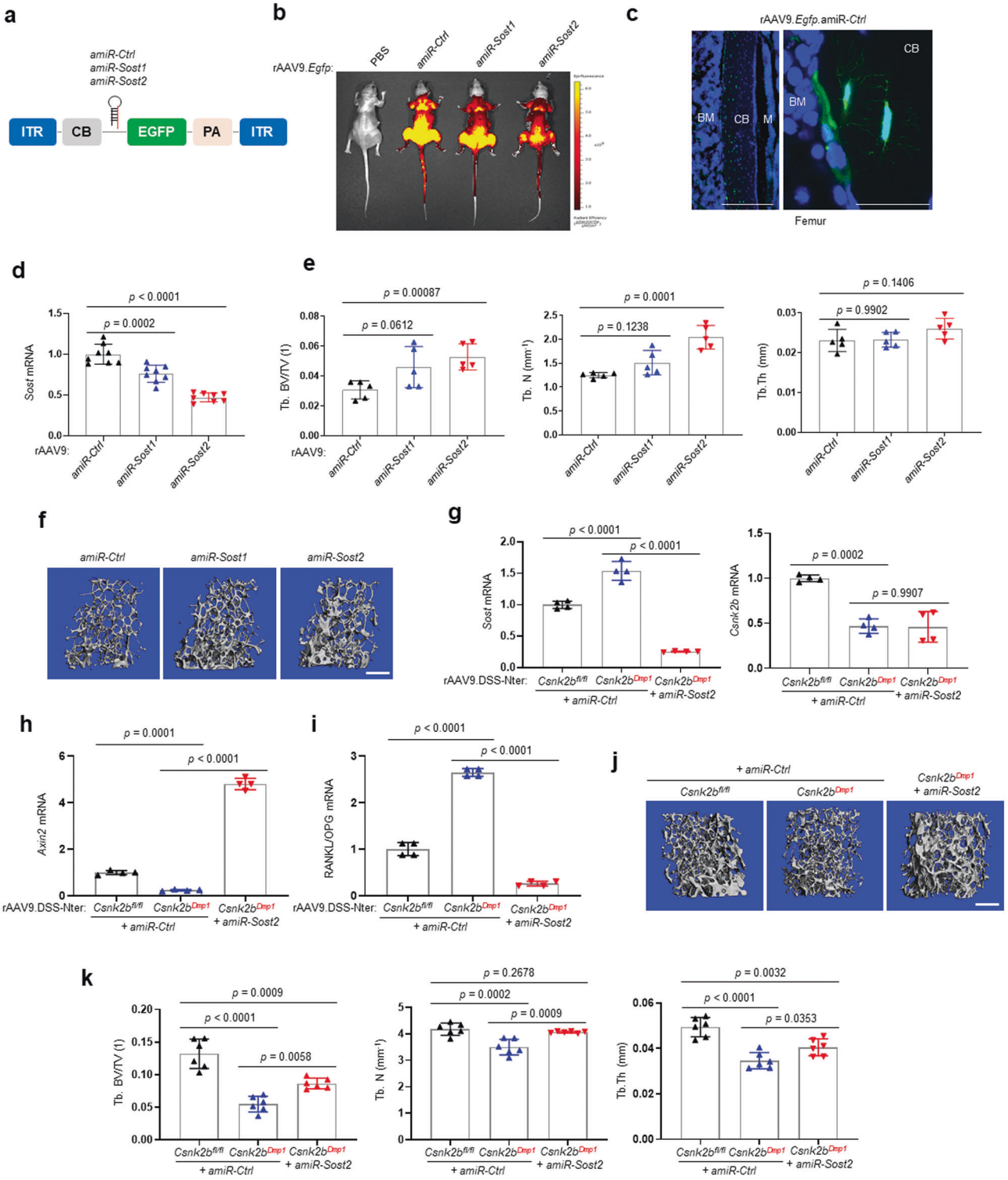

optimization of AAV treatment, such as higher doses of AAV vectors, longer duration of AAV treatment, or AAV treatment at younger age of mice. Alternatively, treatment with anti-sclerostin antibody may be more efficient than AAV-mediated silencing of *Sost*. Additionally, since increased number of osteocytes in *Csnk2b*^{Dmp1} mice is not observed in *SOST*-overexpressing transgenic mice [51], it is possible that the CK2/USP4/SIRT1 pathway may also integrate other signals to regulate osteocyte differentiation and functions, such as calcium/phosphate homeostasis and mechanotransduction, as shown by the differential expression of osteocyte genes in *Csnk2b*-deficient mice and osteocyte culture systems (Supplementary Fig. 4 and 9). A potential role for the CK2/USP4/SIRT1 pathway in osteoporotic fracture or bone loss due to aging, related to upregulated sclerostin level requires more investigations [52]. Additionally, in addition to anti-sclerostin antibody, development of small molecules targeting the CK2/USP4/SIRT1 pathway opens new opportunities to understand how this signal axis plays a role in bone remodeling in vivo and to treat

Fig. 4 Bone-targeting rAAV-mediated silencing of *Sost* reverses osteopenia in *Csnk2b*^{Dmp1} mice. a Diagram of the rAAV9 construct containing a CMV enhancer/chicken β-actin promoter (*CB*), *amiR-ctrl*, *amiR-Sost1*, or *amiR-Sost2*, an *Egfp* reporter gene (*EGFP*), *β-globin* polyA sequence (PA), and inverted terminal repeat (ITR). **b**–**f** rAAV9.egfp carrying *amiR-ctrl, amiR-Sost1*, or *amiR-Sost2* was i.v. injected into 12-week-old wildtype female mice and two months later, EGFP expression was assessed by IVIS 100 optical imaging (**b**) and fluorescence microscopy of cryo-sectioned femurs (**c**). PBS was used for negative control (**b**). Scale bar, 250 μm (**c**, left) and 25 μm (**c**, right). BM bone marrow, M muscle, CB cortical bone. *Sost* mRNA levels in the tibia of AAV-treated mice were assessed by RT-PCR (**d**). MicroCT analysis showing femoral bone mass in AAV-treated mice. Relative quantification (**e**) and representative 3D-reconstruction (**f**) are displayed. Trabecular bone volume/total volume (Tb. BV/TV), trabecular number (Tb. N), and trabecular thickness (Tb.Th) were measured. Scale bar, 500 μm (**f**). **g**–**k** rAAV9.DSS-Nter.egfp carrying *amiR-ctrl* or *amiR-Sost2* was i.v. injected into eight-week-old *Csnk2b*$^{fl/fl}$ and *Csnk2b*^{Dmp1} male mice and two months later, mRNA levels of *Csnk2b*, *Sost* (**g**), *Axin2* (**h**), and a RANKL/OPG ratio (**i**) in the tibia were assessed by RT-PCR. MicroCT analysis showing trabecular bone mass of AAV-treated femurs. Representative 3D-reconstruction (**j**) and relative quantification (**k**) are displayed. Scale bar, 500 μm (**j**). Data are representative of three experiments (**b**–**d**, **f**–**j**) or are pooled from two experiments (**e**, **k**). Ordinary one-way ANOVA with Sidak's multiple comparisons test (**d**, **e**, **g**, **h**, **i**, **k**) or a two-tailed unpaired Student's *t*-test for comparing *amiR-Ctrl*-expressing *Csnk2b*$^{fl/fl}$ mice and *amiR-Sost2*-expressing *Csnk2b*^{Dmp1} mice (**k**) (**d**, **e**, **g**–**i**, **k**; error bars, SD of biological replicates).

skeletal disorders. In this respect, the CK2 inhibitor CX4945 and the SIRT1 activator SRT2104 are under clinical trials for treatment of cancer and inflammatory diseases but have yet to be studied for the treatment of human bone diseases [53, 54].

MATERIALS AND METHODS

Cell lines, plasmids, and antibodies

Ocy454 cells were obtained from Massachusetts General Hospital (MGH, Boston, MA) and maintained in α-MEM medium (Corning) supplemented with 10% FBS (Corning) and 1% penicillin/ streptomycin (Corning) at 33 °C with 5% CO_2. For osteocyte differentiation, cells were transferred to 37 °C when they were confluent at 33 °C and cultured for 6–12 days for the analysis of osteocyte gene expression [27, 55, 56]. HEK293T cells or C3H10T1/2 cells were purchased from ATCC and grown in DMEM (Corning) supplemented with 10% FBS (Corning), 2 mM L-glutamine (Corning), 1% nonessential amino acids (Corning), and 1% penicillin/streptomycin (Corning). All cell lines were regularly tested for mycoplasma contamination. The construct for Flag-*SIRT1* and Flag/HA-*USP22* was deposited to Addgene (#13812) by Eric Verdin and Addgene (#22575) by Wade Harper, respectively. Plasmid for human *USP4* was purchased from DNASU plasmid repository and Flag/HA-*USP4* and Myc-*USP4* were generated by subcloning. The construct for HA-ubiquitin was deposited to Addgene by Edward Yeh (#18712) and plasmid for His-ubiquitin was generated by subcloning. Antibodies specific to CSNK2B (Abclonal, A14722), sclerostin (R&D systems, AF-1589), SIRT1 (Cell signaling, 9475), USP4 (Cell signaling, 2651), P-Ser/Thr (Cell signaling, 9631), P-CK2 substrate (Cell signaling, 8738), USP22 (Novus Biologicals, NBP1-49644SS), Ubiquitin (Santa Cruz Biotechnology, SC-8017), FLAG (Sigma, F1804), and GAPDH (EMD Millipore, CB1001) were used according to manufacturers' instructions. Horse radish peroxidase (HRP)-conjugated anti-rabbit (sc-2357) and anti-mouse (10735086001) secondary antibodies were purchased from Santa Cruz Biotechnology. Recombinant osteoprotegerin (OPG)-Fc fusion were purchased from R&D systems (459-MO). CK2 inhibitor (CK2 inhibitor IV, 218713) and USP4 inhibitor (P22077, MBS577664) were purchased from Calbiochem and Mybiosource, respectively.

Mice

Csnk2b$^{fl/fl}$ mice [26] were previously reported and maintained on C57BL/6 background. 14 kb Dmp1-Cre deleter mouse line and Cre reporter Rosa26$^{mT/mG}$ mice were purchased from the Jackson laboratory. Mouse genotypes were determined by PCR on tail genomic DNA; primer sequences are available upon request. All animals were used in accordance with the NIH Guide for the Care and Use of Laboratory Animals and were handled according to protocols approved by the University of Massachusetts Medical School on animal care (IACUC).

Skeletal analysis

For skeletal analysis, sex-matched and control littermates were used and randomly assigned in all experiments. MicroCT was used for qualitative and quantitative assessment of trabecular and cortical bone microarchitecture and performed by an investigator blinded to the genotypes of the animals under analysis. Femurs excised from the indicated mice were scanned using a microCT 35 (Scanco Medical) with a spatial resolution of 7 μm (Scanning parameters: 55 kVp and114 mA) according to guidelines [57]. For trabecular bone analysis of the distal femur, an upper 2.1 mm region beginning 280 μm proximal to the growth plate was contoured (Segmentation: sigma 0.8, support 1, threshold 280). For cortical bone analysis of femur and tibia, a midshaft region of 0.6 mm in length was used (Segmentation: sigma 0.8, support 1, threshold 350). 3D reconstruction images were obtained from contoured 2D images by methods based on distance transformation of the binarized images. All images presented are representative of the respective genotypes ($n > 5$).

Bone mechanical test

To determine bone mechanical properties, the femoral diaphysis samples of eight-week-old male *Csnk2b*$^{fl/fl}$ and *Csnk2b*^{Dmp1} mice were used. Briefly, femora were mechanically tested in three-point bending using an electrical force materials testing machine (Electroforce 3230, Bose Corporation, Eden Prairie, MN) at the Center for Skeletal Research Imaging and Biomechanical Testing Core in MGH. The bending fixture had a bottom span length of 8 mm. The test was performed with the load point in displacement control moving at a rate of 0.1 mm/sec with force and displacement data collected at 60 Hz. All of the bones were positioned in the same orientation during testing with femoral diaphysis resting on the supports and being loaded in tension. Bending rigidity (EI, N-mm2), work to maximum moment (mJ), and maximum moment (Nmm) were calculated based on the force and displacement data from the tests and the mid-shaft geometry measured with microCT. Work to fracture is the energy that that was required to cause the femur to fracture, and it was calculated by finding the area under the force-displacement curve using the Riemann Sum method.

Histology, histomorphometry, immunohistochemistry, and immunofluorescence

All experiments for histology, histomorphometry, and immunohistochemistry were performed based on previous publication with modifications [24]. Briefly, for histological analysis, femurs were dissected from the mice, fixed in 10% neutral buffered formalin for 2 days, and decalcified by every two day changes of 0.5 M tetrasodium EDTA for 3–4 weeks. Tissues were dehydrated by passage through an ethanol series, cleared twice in xylene, embedded in paraffin, and sectioned at 7 μm thickness along the coronal plate from anterior to posterior. Decalcified femoral sections were stained with hematoxylin and eosin (H&E) or tartrate-resistant acid phosphatase (TRAP).

For histomorphometric analysis, 25 mg/kg calcein (Sigma, C0875) and 50 mg/kg alizarin-3-methyliminodiacetic acid (Sigma, A3882) dissolved in 2% $NaHCO_3$ solution were intraperitoneally injected into eight-week-old male mice at four-day-interval. After two days of fixation in 10% neutral buffered formalin, undecalcified femur samples were embedded in methylmethacrylate. Proximal metaphysis was sectioned longitudinally (5 μm) and stained with toluidine blue for osteocytes and osteolasts [58]. A region of interest is defined in the trabecular bone in the metaphysis and bone formation rate/bone surface (BFR/BS), mineral apposition rate (MAR), osteocyte number/bone area (N.Ot/B.Ar), osteoclast number/bone perimeter (N.Oc/B.Pm), and osteoclast surface/bone surface (Oc.S/BS) were measured using a semiautomatic analysis system (OsteoMetrics, Atlanta, GA, USA). Measurements are taken on two sections/sample (separated by ~25 μm) and summed prior to normalization to obtain a single measure/sample in accordance with ASBMR standards [59, 60]. This methodology has undergone extensive quality control and validation and the results were assessed by a research specialist in a blinded fashion.

For immunohistochemistry, paraffin sections were deparaffinized and hydrated. Citrate-based solution (VECTOR, H3300) and 3% H_2O_2/MeOH were used for antigen retrieval and quenching, respectively. After Sections were incubated with antibodies specific CSNK2B (1:100, Abclonal, A14722), sclerostin

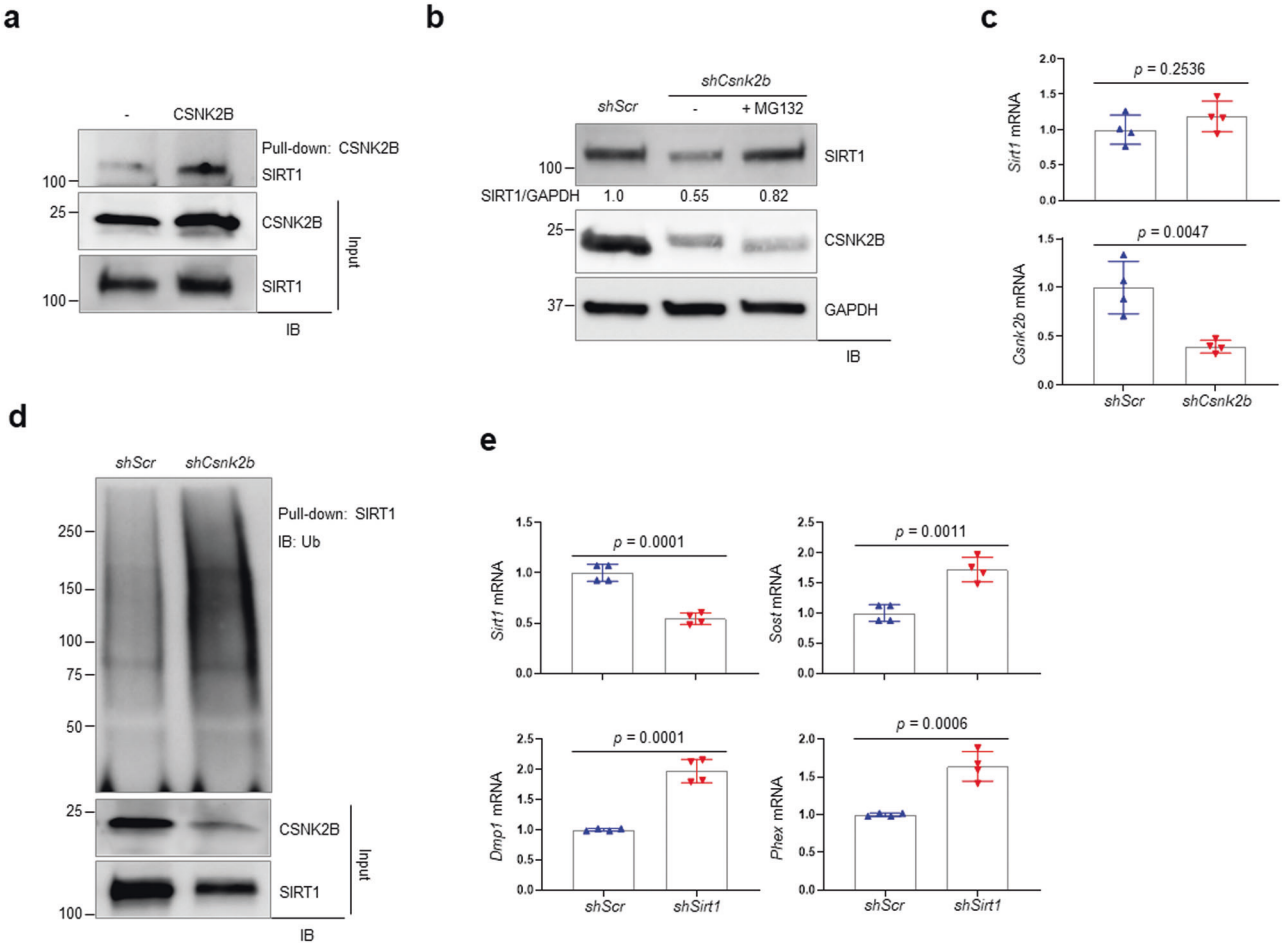

Fig. 5 CK2 controls the stability of SIRT1 in osteocytes. a Ocy454 cells were transfected with vector or Myc-*CSNK2B* and 48 h later, cell lysates were pull-downed with Myc-conjugated agarose and immunoblotted with the indicated antibodies. **b** Immunoblot analysis showing protein levels of SIRT1 in *shScr* or *shCsnk2b*-expressing Ocy454 cells six days after differentiation. Alternatively, cells were treated with 10 μM MG132 for 6 h before harvest. SIRT1/GAPDH, a ratio of relative density of SIRT1 protein expression to GAPDH. (c) mRNA levels of *Sirt1* and *Csnk2b* in *shScr* or *shCsnk2b*-expressing Ocy454 cells were assessed by RT-PCR ($n = 4$/group). **d** *shScr* or *shCsnk2b*-expressing Ocy454 cells were transfected with Flag-*SIRT1* and HA-ubiquitin and 48 h later, cells were treated with 10 μM MG132 for 6 h, pull-downed with Flag-conjugated agarose, and immunoblotted with anti-ubiquitin (Ub) antibody. **e** mRNA levels of osteocyte genes in *shScr* or *shSirt1*-expressing Ocy454 cells 6 days after differentiation were assessed by RT-PCR ($n = 4$/group). Data are representative of three. A two-tailed unpaired Student's *t*-test for comparing two groups (**c**, **e**; error bars, SD of biological replicates).

(1:100, R&D systems, AF-1589) or cathepsin k (1:100, Abclonal, A1782) for 40 min at 37 °C, and secondary antibodies for 20 min at 37 °C. Subsequently, they were incubated in streptavidin-horseradish peroxidase (SA-HRP) for 16 min at 37 °C and then 3,3′-Diaminobenzidine (DAB) + H_2O_2 substrate for 8 min followed by hematoxylin and bluing reagent counterstain at 37 °C.

For immunofluorescence, femoral bone was fixed with 4% paraformaldehyde (PFA) for two days and decalcified in 0.5 M tetrasodium EDTA solution for 10 days. Semi-decalcified samples were infiltrated with 25% sucrose phosphate for four days. All samples were embedded in 50/50 mixture of 25% sucrose solution and optimal cutting temperature (OCT, a water-soluble blend of glycols and resins) compound (Sakura) and cut into 12-μm-thick sagittal sections using a cryostat (Leica). Eight-week-old mouse cryosectioned femoral samples were stained with antibodies for CSNK2B (1:100, Santa Cruz Biotechnology, sc-12739 AF488), osteocalcin (1:100, Abclonal, A6205), and sclerostin (1:100, R&D systems, AF-1589). Cryosectioned femurs of 8-week-old *Dmp1;Rosa26*$^{mT/mG}$ mice were stained for CSNK2B (1:100, Abclonal, A14722). Alexa Fluor 594 (1:400, Thermo, A11032) was used as a secondary antibody for both experiments. Nuclei were stained with 4–6, diamidino-2-phenylindole (DAPI). An Olympus IX81confocal microscope was used to image samples.

Detection of RANKL and CTx-I

Mouse serum levels of RANKL (R&D systems, MTR00) or CTx-I (Immunodiagnostic Systems, AC-06F1) were measured according to manufacturers' protocols.

Culture of osteocyte-enriched fraction

The osteocyte-enriched bone fraction was obtained from femurs and tibias from eight-week-old male mice as previously described [16]. Briefly, bone marrow cells were removed from femurs and tibias and remaining bone pieces were digested by sequential 2 mg/ml collagenase type II in α-MEM medium and 5 mM EDTA in PBS. After incubation, cells were collected, passed through a 70 μm nylon mesh and cultured in α-MEM supplemented with 10% FBS and 1% penicillin/ streptomycin. After 28 days of culture, cellular morphology was determined by phalloidin staining (Biotium, CF568) and Hoechst (Abcam, ab228551).

Collection of conditioned medium from WT and *Csnk2b*-deficient osteocytes

Conditioned medium (CM) from *shScr*- and *shCsnk2b*-expressing osteocytes was collected six days after osteocyte differentiation. Cells were washed with cold PBS three times to remove residual serum from the culture medium and incubated with serum free α-MEM for 48 h. Each CM sample was collected and filtered with 0.45 μm syringe filter to remove cellular debris.

Osteoblast differentiation

Primary calvarial osteoblasts (COBs) were isolated from calvarium of five-day-old *Csnk2b*$^{fl/fl}$ neonates using collagenase type II (50 mg/ml, Worthington,

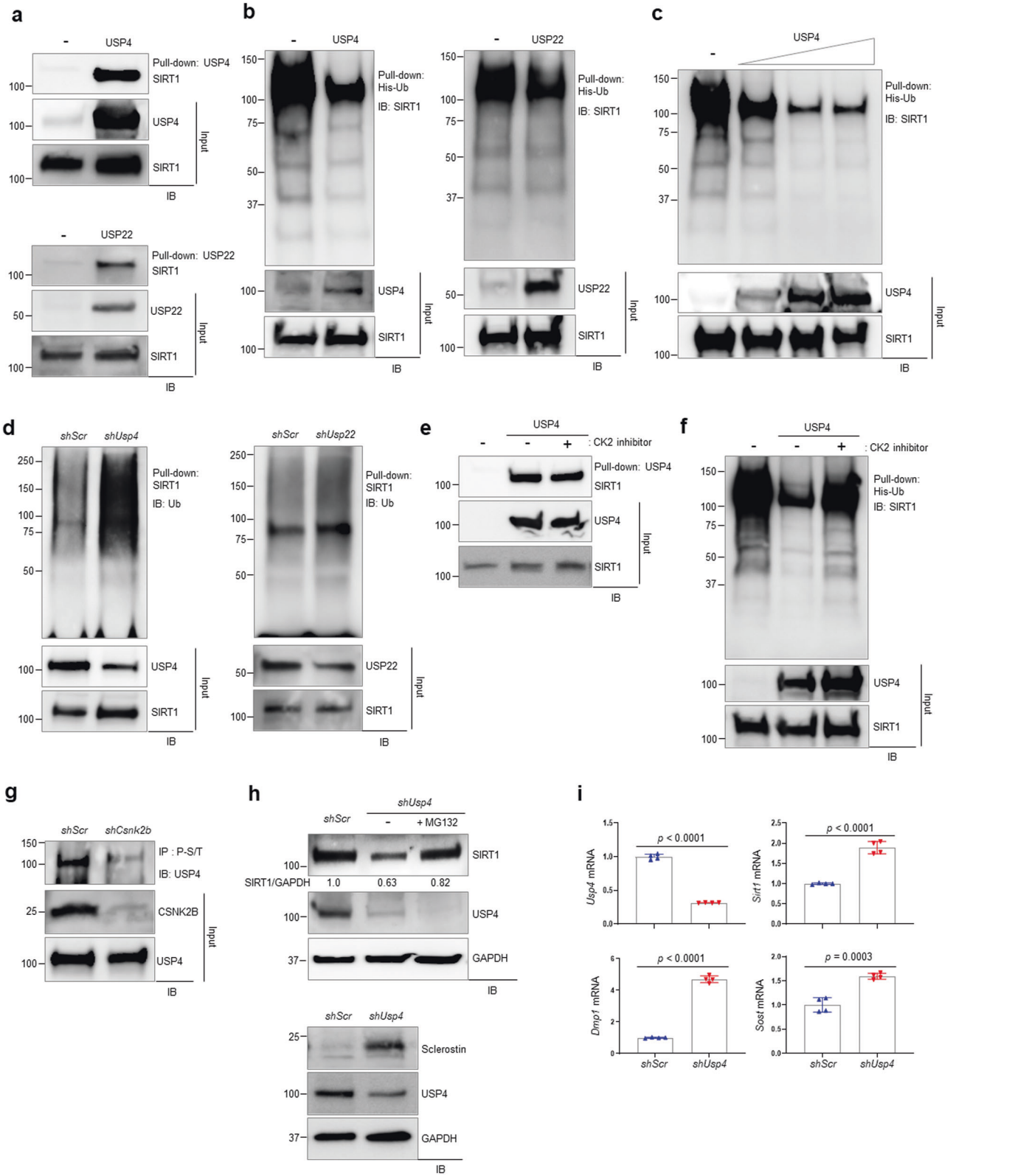

LS004176)/dispase II (100 mg/ml, Roche, 10165859001). *Csnk2b*$^{fl/fl}$ COBs were transduced with either lentiviruses expressing EGFP (control) or CRE-recombinase. At 48 h after infection, cells were treated with puromycin for selection. COBs were maintained in α-MEM medium (Gibco) containing 10% FBS (Gibco), 2 mM L-glutamine (Corning), 1% penicillin/ streptomycin (Corning) and 1% nonessential amino acids (Corning). Bone marrow stromal cells (BMSCs) were isolated from crushed long bones of eight-week-old mice and cultured under non-osteogenic medium (α-MEM medium (Gibco), 10% FBS, 2 mM L-glutamine, 1% nonessential amino acids, and 1% penicillin/ streptomycin). For osteogenic differentiation, ascorbic acid (200 uM, Sigma, A8960) and β-glycerophosphate (10 mM, Sigma, G9422) were added to non-osteogenic medium. For alkaline phosphatase (ALP) activity assay,

Fig. 6 CK2-mediated phosphorylation of USP4 controls SIRT1 stabilization. a HEK293T cells were transfected with Flag/HA-tagged *USP4* or *USP22* along with HA-ubiquitin. After 48 h of transfection, cells were treated with 10 μM MG132 for 6 h, lysed, pull-downed with Flag-conjugated agarose, and immunoblotted. **b** HEK293T cells were transfected with Flag/HA-tagged *USP4*, or *USP22* along with *SIRT1* and His-ubiquitin. After 48 h of transfection, cells were treated with 10 μM MG132 for 6 h, lysed, pull-downed with Ni-NTA agarose, and immunoblotted with anti-SIRT1 antibody. **c** Flag-*SIRT1* and His-ubiquitin were transfected into HEK293T cells along with different concentrations of Myc-*USP4*. Two days after transfection, cells were treated with 10 μM MG132 for 6 h, lysed, pull-downed with Ni-NTA agarose, and immunoblotted with anti-SIRT1 antibody. **d** *shScr*, *shUsp4*, or *shUsp22*-expressing Ocy454 cells were transfected with Flag-*SIRT1* and HA-ubiquitin. After 48 h of transfection, cells were treated with 10 μM MG132 for 6 h, lysed, pull-downed with Flag-conjugated agarose, and immunoblotted with anti-ubiquitin antibody. **e**, **f** HEK293T cells were transfected with Flag-*USP4* and HA-ubiquitin (**e**) or Myc-*USP4*, Flag-*SIRT1* and His-ubiquitin (**f**) in the absence or presence of 1 μM CK2 inhibitor. After 48 h of transfection, cells were treated with 10 μM MG132 for 6 h, lysed, pull-downed with Flag-conjugated agarose (**e**) or Ni-NTA agarose (**f**), and immunoblotted. **g** *shScr* or *shCsnk2b*-expressing Ocy454 cells were lysed, immunoprecipitated with anti-phospho-ser/thr antibody (P-S/T), and immunoblotted for USP4. **h** *shScr* or *shUsp4*-expressing Ocy454 cells were cultured in osteocyte differentiation condition for 12 days in the presence of 1 μM CK2 inhibitor and protein lysates were immunoblotted with indicated antibodies. Alternatively, cells were treated with 10 μM MG132 for 6 h. SIRT1/GAPDH, a ratio of relative density of SIRT1 protein expression to GAPDH. **i** *shScr* or *shUsp4*-expressing Ocy454 cells were cultured in osteocyte differentiation condition for six days and osteocyte gene expression was examined by RT-PCR. Data are representative of two or three independent experiments (**a**–**i**). A two-tailed unpaired Student's *t*-test for comparing two groups (i; error bars, SD of biological replicates).

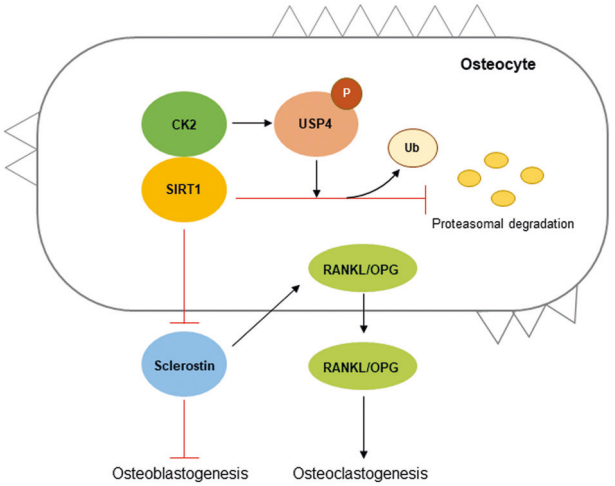

Fig. 7 Schematic diagram depicting a molecular mechanism by which the CK2/USP4/SIRT1 signaling axis controls sclerostin expression in osteocytes. CK2-induced USP4 phosphorylation mediates the deubiquitination of SIRT1 and stabilization of SIRT1. Upregulation of SIRT1 downregulates sclerostin expression in osteocytes and decreases a RANKL/OPG ratio, which decreases osteoclastogenesis and increases osteoblastogenesis simultaneously.

osteoblasts were incubated with Alamar Blue solution (Invitrogen, DAL1100) to check cell viability. Subsequently, cells were washed with PBS and incubated with a solution containing 6.5 mM Na_2CO_3, 18.5 mM $NaHCO_3$, 2 mM $MgCl_2$, and phosphatase substrate (Sigma, S0942), and ALP activity was measured by spectrometer.

Osteoclast differentiation

For osteoclast culture, bone marrow-derived monocytes (BMMs) were collected by flushing bone marrow cells from the femur and tibia of 8-week-old mice. Cells were plated and next day, non-adherent cells were transferred to a new plate and cultured in the presence of M-CSF (30 ng/ml, R&D systems, 416-ML). When cells reach to 80% confluency, cells were treated with M-CSF (30 ng/ml) and RANKL (10 ng/ml, R&D systems, 462-TEC) for osteoclast differentiation. Tartrate-resistant acid phosphatase (TRAP) staining was performed and the enzyme activity were measured for osteoclast differentiation. TRAP staining was performed according to manufacturer's protocol (Sigma, 387 A). For TRAP activity assay, 50 μl of culture supernatant collected from BMM culture was incubated with a mixture (150 μl) of 0.1 M acetate solution (Sigma, 3863), 90 mM $C_4H_4Na_2O_6$, and 7.6 mM p-nitrophenyl phosphate (p-NPP) at 37 °C for 1 h. After then, 50 μl of 3 N NaOH was added and measured at 405 nm by spectrometer.

Transcriptome analysis of Ocy454 cells

shScr- or *shCsnk2b*-expressing Ocy454 cells were cultured under osteocyte differentiation condition (at 37 °C) for six days and samples were subjected for bulk RNA sequencing analysis. For transcriptome analysis, three samples per each group (*shScr* vs. *shCsnk2b*) were mapped to the mouse reference genome (Mus_musculus.GRCm38.101) with STAR aligner (v.2.6.1b) [61, 62]. After mapping, read counts were generated by using HTSeq-count (v.0.11.3) [63]. The read counts were used for a differential expression analysis between *shScr*- or *shCsnk2b*-expresing Ocy454 cells using DESeq2 (v.1.28.1) [64] with the ashr shrinkage estimator (v.2.2.47) [65]. Statistically significantly expressed genes were determined as having absolute log-fold change larger than 1.2 and having a P-value less than 0.005.

Luciferase reporter assay

β-catenin-responsive reporter gene (TopFlash-luc) and *Renilla* luciferase vector (Promega, Madison, WI) were transfected into C3H10T1/2 cells using the Effectene transfection reagent (Qiagen). After 48 h, dual luciferase assay was performed according to the manufacturer's protocol (Promega) and TopFlash luciferase activity was normalized to *Renilla*.

rAAV vector design and production

Bone-targeting AAV9 vectors were generated as described in previous studies [34, 35]. DNA sequences for *amiR-33-Ctrl*, *amiR-33-sost1, and amiR-33-sost2* were synthesized as gBlocks and cloned into the intronic region of the pAAVsc-*CB6-Egfp* plasmid at the restriction enzyme sites (PstI and BglII) [66]. The pAAV-*amiR-Ctrl*, pAAV-*amiR-Sost1*, and pAAV-*amiR-Sost2* constructs were packaged into AAV9 capsid or the bone-targeting AAV9 capsid (AAV9.DSS.N-ter). rAAV production was performed by transient transfection of HEK293 cells, purified by CsCl sedimentation, titrated by droplet digital PCR (ddPCR) on a QX200 ddPCR system (Bio-Rad) using the Egfp prime/probe set as previously described3. The sequences of gBlocks and oligonucleotides for ddPCR and are listed in Supplementary Table 1.

RT-PCR, immunoblotting, and pull-down assay

To prepare bone RNA samples from the mouse limbs, the hindlimbs were dissected and skin/muscle tissues were removed. The remaining tibias were chopped and homogenized. Total RNAs from cells or tissues were extracted using QIAzol (QIAGEN) and cDNA was synthesized using the High-Capacity cDNA Reverse Transcription Kit from Applied Biosystems. Quantitative RT-PCR was performed using SYBR® Green PCR Master Mix (Bio-Rad, Hercules, CA) with Bio-Rad CFX Connect Real-Time PCR detection system. Ribosomal protein, large, P0 (*Rplp0*) was used for housekeeping gene. The primers used for PCR are described in the Supplementary Table 2.

To examine the interaction between CSNK2B and SIRT1, Ocy454 cells were transfected with 1 ug of control or Myc-*CSNK2B* DNA construct using the Effectene transfection reagent for 48 h, and cell lysates were prepared in lysis buffer (50 mM Tris-HCl (pH 7.8), 150 mM NaCl, 1% Triton X-100, 1 mM dithiothreitol (DTT), 0.2% Sarkosyl acid and protease inhibitor cocktail (Sigma, P8340)). Cell lysates were incubated with 40 ul of Myc-conjugated agarose (Santa Cruz Biotechnology, SC-40AC) at 4 °C overnight (12-16 h), and subjected to SDS-PAGE. To screen deubiquitinating enzymes (DUBs) that bind to SIRT1, HEK293T cells were transfected with a panel of Flag-tagged DUBs (1 ug): ubiquitin-specific peptidase family (USP 1, 2, 4, 6, 7, 8, 11, 13, 14, 15, 21, 39), ovarian tumor domain-containing deubiquitinase family (OTUD 1,

4, 5, 6B), Josephin (JOSD1, 2) with HA-ubiquitin (1 ug) using the Effectene for 48 h, cell lysates were pull-downed with 40 ul of Flag-conjugated agarose (Sigma, A2220) at 4 °C overnight (12–16 h) and subjected to SDS-PAGE. To examine USP4 phosphorylation in the absence of *Csnk2b*, cell lysates from *shScr*- or *shCsnk2b*-expressing Ocy454 cells were incubated with anti-P-Ser/Thr antibody at 4 °C overnight, pull-downed with protein G-conjugated agarose (Sigma, P3296) at 4 °C for 4 h, and subjected to SDS-PAGE. Protein samples transferred to Immobilon-P membranes (Millipore) were immunoblotted with the indicated antibodies and developed with ECL (Thermoscientific). Immunoblotting with antibody specific to GAPDH was used as a loading control. All primary antibodies used for immunoblotting were diluted (1:1000) in 1X Tris Buffered Saline with Tween 20 (TBST) solution (137 mM Sodium Chloride, 20 mM Tris, 0.1% Tween-20, pH 7.4) that contained 5% bovine serum albumin (BSA, Roche, 10735086001). All secondary antibodies for immunoblotting were diluted (1:1000) in 1X TBST buffer that contained 5% skimmed milk. All uncropped and unmodified immunoblot images are included in Supplementary Data.

Ubiquitination/deubiquitination assay

For ubiquitination assay, control, *Csnk2b*-deficient or *Usp4*-deficient Ocy454 cells were transfected with 1 ug Flag-*SIRT1* and 1 ug HA-ubiquitin-expressing plasmids. After 48 h, cells were treated with 10 μM MG132 (EMD-Millipore, 474790) for 6 h, and pulled-down with Flag-conjugated agarose (Sigma, A2220) at 4 °C overnight. The pull-down samples were subjected to SDS-PAGE and immunoblotted with anti-ubiquitin antibody. To test the ability of USP4 or USP22 to deubiquitinate ubiquitinated SIRT1, plasmid expressing Flag-*SIRT1* (1 ug) was transfected into HEK293T cells along with His-ubiquitin-expressing plasmid (1 ug) in the absence or presence of *USP4* or *USP22*-expressing plasmid (1 ug). After 48 h, cells were treated with 10 μM MG132 for 6 h, lysed and sonicated in denaturation buffer (8 M urea, 50 mM tris pH 8.0, 1.0% triton X-100, 10 mM imidazole, 10 mM β-mercaptoethanol), and pulled-down with 40 ul of Ni-NTA beads (Qiagen, 30210) at room temperature overnight. The pull-down samples were subjected to SDS-PAGE and immunoblotted with anti-SIRT1 antibody.

Statistics and reproducibility

All experiments were carried out at least two or three times, for IHC, histological staining, and immunoblotting, representative images are shown. All data are shown as the mean ± Standard Deviation (SD). We first performed the Shapiro–Wilk normality test for checking normal distributions of the groups. If normality tests passed, two-tailed, unpaired Student's *t*-test and if normality tests failed, and Mann–Whitney tests were used for the comparisons between two groups. For the comparisons of three groups, we used one-way ANOVA if normality tests passed, followed by Tukey's multiple comparison test for all pairs of groups. The GraphPad PRISM software (ver.9.0.2, La Jolla, CA) was used for statistical analysis. $P < 0.05$ was considered statistically significant.

DATA AVAILABILITY

Data supporting the findings of this manuscript are available from the corresponding author upon reasonable request.

REFERENCES

1. Sims NA, Martin TJ. Osteoclasts provide coupling signals to osteoblast lineage cells through multiple mechanisms. Annu Rev Physiol. 2020;82:507–29.
2. Kim JM, Lin C, Stavre Z, Greenblatt MB, Shim JH. Osteoblast-osteoclast communication and bone homeostasis. Cells. 2020;9:2073.
3. Robling AG, Bonewald LF. The osteocyte: new insights. Annu Rev Physiol. 2020;82:485–506.
4. Bonewald LF. The amazing osteocyte. J Bone Min Res. 2011;26:229–38.
5. Plotkin LI, Bellido T. Osteocytic signalling pathways as therapeutic targets for bone fragility. Nat Rev Endocrinol. 2016;12:593–605.
6. Xiong J, Onal M, Jilka RL, Weinstein RS, Manolagas SC, O'Brien CA. Matrix-embedded cells control osteoclast formation. Nat Med. 2011;17:1235–41.
7. van Bezooijen RL, Roelen BA, Visser A, van der Wee-Pals L, de Wilt E, Karperien M, et al. Sclerostin is an osteocyte-expressed negative regulator of bone formation, but not a classical BMP antagonist. J Exp Med. 2004;199:805–14.
8. Baron R, Kneissel M. WNT signaling in bone homeostasis and disease: from human mutations to treatments. Nat Med. 2013;19:179–92.
9. Brunkow ME, Gardner JC, Van Ness J, Paeper BW, Kovacevich BR, Proll S, et al. Bone dysplasia sclerosteosis results from loss of the SOST gene product, a novel cystine knot-containing protein. Am J Hum Genet. 2001;68:577–89.
10. Balemans W, Patel N, Ebeling M, Van Hul E, Wuyts W, Lacza C, et al. Identification of a 52 kb deletion downstream of the SOST gene in patients with van Buchem disease. J Med Genet. 2002;39:91–7.
11. Loots GG, Kneissel M, Keller H, Baptist M, Chang J, Collette NM, et al. Genomic deletion of a long-range bone enhancer misregulates sclerostin in Van Buchem disease. Genome Res. 2005;15:928–35.
12. Collette NM, Genetos DC, Economides AN, Xie L, Shahnazari M, Yao W, et al. Targeted deletion of Sost distal enhancer increases bone formation and bone mass. Proc Natl Acad Sci USA. 2012;109:14092–7.
13. Li X, Ominsky MS, Niu QT, Sun N, Daugherty B, D'Agostin D, et al. Targeted deletion of the sclerostin gene in mice results in increased bone formation and bone strength. J Bone Min Res. 2008;23:860–9.
14. Cohen-Kfir E, Artsi H, Levin A, Abramowitz E, Bajayo A, Gurt I, et al. Sirt1 is a regulator of bone mass and a repressor of Sost encoding for sclerostin, a bone formation inhibitor. Endocrinology 2011;152:4514–24.
15. Zainabadi K. Drugs targeting SIRT1, a new generation of therapeutics for osteoporosis and other bone related disorders? Pharm Res. 2019;143:97–105.
16. Stegen S, Stockmans I, Moermans K, Thienpont B, Maxwell PH, Carmeliet P, et al. Osteocytic oxygen sensing controls bone mass through epigenetic regulation of sclerostin. Nat Commun. 2018;9:2557.
17. Simic P, Zainabadi K, Bell E, Sykes DB, Saez B, Lotinun S, et al. SIRT1 regulates differentiation of mesenchymal stem cells by deacetylating beta-catenin. EMBO Mol Med. 2013;5:430–40.
18. Mercken EM, Mitchell SJ, Martin-Montalvo A, Minor RK, Almeida M, Gomes AP, et al. SRT2104 extends survival of male mice on a standard diet and preserves bone and muscle mass. Aging Cell. 2014;13:787–96.
19. Ahmed K, Gerber DA, Cochet C. Joining the cell survival squad: an emerging role for protein kinase CK2. Trends Cell Biol. 2002;12:226–30.
20. Niefind K, Guerra B, Ermakowa I, Issinger OG. Crystal structure of human protein kinase CK2: insights into basic properties of the CK2 holoenzyme. EMBO J. 2001;20:5320–31.
21. Litchfield DW. Protein kinase CK2: structure, regulation and role in cellular decisions of life and death. Biochem J. 2003;369:1–15.
22. Buchou T, Vernet M, Blond O, Jensen HH, Pointu H, Olsen BB, et al. Disruption of the regulatory beta subunit of protein kinase CK2 in mice leads to a cell-autonomous defect and early embryonic lethality. Mol Cell Biol. 2003;23:908–15.
23. Lou DY, Dominguez I, Toselli P, Landesman-Bollag E, O'Brien C, Seldin DC. The alpha catalytic subunit of protein kinase CK2 is required for mouse embryonic development. Mol Cell Biol. 2008;28:131–9.
24. Kim JM, Yang YS, Park KH, Ge X, Xu R, Li N, et al. A RUNX2 stabilization pathway mediates physiologic and pathologic bone formation. Nat Commun. 2020;11:2289.
25. Lu Y, Xie Y, Zhang S, Dusevich V, Bonewald LF, Feng JQ. DMP1-targeted Cre expression in odontoblasts and osteocytes. J Dent Res. 2007;86:320–5.
26. Ulges A, Klein M, Reuter S, Gerlitzki B, Hoffmann M, Grebe N, et al. Protein kinase CK2 enables regulatory T cells to suppress excessive TH2 responses in vivo. Nat Immunol. 2015;16:267–75.
27. Spatz JM, Wein MN, Gooi JH, Qu Y, Garr JL, Liu S, et al. The Wnt inhibitor sclerostin is up-regulated by mechanical unloading in osteocytes in vitro. J Biol Chem. 2015;290:16744–58.
28. Poole KE, van Bezooijen RL, Loveridge N, Hamersma H, Papapoulos SE, Lowik CW, et al. Sclerostin is a delayed secreted product of osteocytes that inhibits bone formation. FASEB J. 2005;19:1842–4.
29. Maurel DB, Matsumoto T, Vallejo JA, Johnson ML, Dallas SL, Kitase Y, et al. Characterization of a novel murine Sost ER(T2) Cre model targeting osteocytes. Bone Res. 2019;7:6.
30. Tu X, Rhee Y, Condon KW, Bivi N, Allen MR, Dwyer D, et al. Sost downregulation and local Wnt signaling are required for the osteogenic response to mechanical loading. Bone 2012;50:209–17.
31. Tu X, Delgado-Calle J, Condon KW, Maycas M, Zhang H, Carlesso N, et al. Osteocytes mediate the anabolic actions of canonical Wnt/beta-catenin signaling in bone. Proc Natl Acad Sci USA. 2015;112:E478–86.
32. Wijenayaka AR, Kogawa M, Lim HP, Bonewald LF, Findlay DM, Atkins GJ. Sclerostin stimulates osteocyte support of osteoclast activity by a RANKL-dependent pathway. PLoS One. 2011;6:e25900.
33. Allison H, Holdsworth G, McNamara LM. Scl-Ab reverts pro-osteoclastogenic signalling and resorption in estrogen deficient osteocytes. BMC Mol Cell Biol. 2020;21:78.
34. Yang YS, Xie J, Wang D, Kim JM, Tai PWL, Gravallese E, et al. Bone-targeting AAV-mediated silencing of Schnurri-3 prevents bone loss in osteoporosis. Nat Commun. 2019;10:2958.

35. Yang YS, Xie J, Chaugule S, Wang D, Kim JM, Kim J, et al. Bone-targeting AAV-mediated gene silencing in osteoclasts for osteoporosis therapy. Mol Ther Methods Clin Dev. 2020;17:922–35.
36. Sasaki T, Maier B, Koclega KD, Chruszcz M, Gluba W, Stukenberg PT, et al. Phosphorylation regulates SIRT1 function. PLoS One. 2008;3:e4020.
37. Revollo JR, Li X. The ways and means that fine tune Sirt1 activity. Trends Biochem Sci. 2013;38:160–7.
38. Pinna LA. Protein kinase CK2: a challenge to canons. J Cell Sci. 2002;115(Pt 20):3873–8.
39. Lin Z, Yang H, Kong Q, Li J, Lee SM, Gao B, et al. USP22 antagonizes p53 transcriptional activation by deubiquitinating Sirt1 to suppress cell apoptosis and is required for mouse embryonic development. Mol Cell. 2012;46:484–94.
40. Meggio F, Pinna LA. One-thousand-and-one substrates of protein kinase CK2? FASEB J. 2003;17:349–68.
41. Zhang L, Zhou F, Drabsch Y, Gao R, Snaar-Jagalska BE, Mickanin C, et al. USP4 is regulated by AKT phosphorylation and directly deubiquitylates TGF-beta type I receptor. Nat Cell Biol. 2012;14:717–26.
42. Das T, Shin SC, Song EJ, Kim EE. Regulation of deubiquitinating enzymes by post-translational modifications. Int J Mol Sci. 2020;21:4028.
43. Zschoernig B, Mahlknecht U. Carboxy-terminal phosphorylation of SIRT1 by protein kinase CK2. Biochem Biophys Res Commun. 2009;381:372–7.
44. Kang H, Jung JW, Kim MK, Chung JH. CK2 is the regulator of SIRT1 substrate-binding affinity, deacetylase activity and cellular response to DNA-damage. PLoS One. 2009;4:e6611.
45. Li Q, Cheng JC, Jiang Q, Lee WY. Role of sirtuins in bone biology: potential implications for novel therapeutic strategies for osteoporosis. Aging Cell. 2021;20:e13301.
46. Zainabadi K, Liu CJ, Guarente L. SIRT1 is a positive regulator of the master osteoblast transcription factor, RUNX2. PLoS One. 2017;12:e0178520.
47. Gurt I, Artsi H, Cohen-Kfir E, Hamdani G, Ben-Shalom G, Feinstein B, et al. The Sirt1 Activators SRT2183 and SRT3025 Inhibit RANKL-Induced Osteoclastogenesis in Bone Marrow-Derived Macrophages and Down-Regulate Sirt3 in Sirt1 Null Cells. PLoS One. 2015;10:e0134391.
48. Zhou F, Li F, Fang P, Dai T, Yang B, van Dam H, et al. Ubiquitin-specific protease 4 antagonizes osteoblast differentiation through dishevelled. J Bone Min Res. 2016;31:1888–98.
49. Yun SI, Kim HH, Yoon JH, Park WS, Hahn MJ, Kim HC, et al. Ubiquitin specific protease 4 positively regulates the WNT/beta-catenin signaling in colorectal cancer. Mol Oncol. 2015;9:1834–51.
50. Kushioka J, Kaito T, Okada R, Ishiguro H, Bal Z, Kodama J, et al. A novel negative regulatory mechanism of Smurf2 in BMP/Smad signaling in bone. Bone Res. 2020;8:41.
51. Delgado-Calle J, Sato AY, Bellido T. Role and mechanism of action of sclerostin in bone. Bone 2017;96:29–37.
52. Ardawi MS, Al-Kadi HA, Rouzi AA, Qari MH. Determinants of serum sclerostin in healthy pre- and postmenopausal women. J Bone Min Res. 2011;26:2812–22.
53. D'Amore C, Borgo C, Sarno S, Salvi M. Role of CK2 inhibitor CX-4945 in anti-cancer combination therapy - potential clinical relevance. Cell Oncol (Dordr). 2020;43:1003–16.
54. Dai H, Sinclair DA, Ellis JL, Steegborn C. Sirtuin activators and inhibitors: promises, achievements, and challenges. Pharm Ther. 2018;188:140–54.
55. Wein MN, Spatz J, Nishimori S, Doench J, Root D, Babij P, et al. HDAC5 controls MEF2C-driven sclerostin expression in osteocytes. J Bone Min Res. 2015;30:400–11.
56. Gould NR, Williams KM, Joca HC, Torre OM, Lyons JS, Leser JM, et al. Disparate bone anabolic cues activate bone formation by regulating the rapid lysosomal degradation of sclerostin protein. Elife. 2021;10:e64393.
57. Bouxsein ML, Boyd SK, Christiansen BA, Guldberg RE, Jepsen KJ, Muller R. Guidelines for assessment of bone microstructure in rodents using micro-computed tomography. J Bone Min Res. 2010;25:1468–86.
58. Fukuda T, Takeda S, Xu R, Ochi H, Sunamura S, Sato T, et al. Sema3A regulates bone-mass accrual through sensory innervations. Nature 2013;497:490–3.
59. Parfitt AM, Drezner MK, Glorieux FH, Kanis JA, Malluche H, Meunier PJ, et al. Bone histomorphometry: standardization of nomenclature, symbols, and units. Report of the ASBMR Histomorphometry Nomenclature Committee. J Bone Min Res. 1987;2:595–610.
60. Dempster DW, Compston JE, Drezner MK, Glorieux FH, Kanis JA, Malluche H, et al. Standardized nomenclature, symbols, and units for bone histomorphometry: a 2012 update of the report of the ASBMR histomorphometry nomenclature committee. J Bone Min Res. 2013;28:2–17.
61. Dobin A, Davis CA, Schlesinger F, Drenkow J, Zaleski C, Jha S, et al. STAR: ultrafast universal RNA-seq aligner. Bioinformatics 2013;29:15–21.
62. Dobin A, Gingeras TR. Mapping RNA-seq reads with STAR. Curr Protoc Bioinforma 2015;51:11.4. 1–4. 9.
63. Anders S, Pyl PT, Huber W. HTSeq—a Python framework to work with high-throughput sequencing data. Bioinformatics 2015;31:166–9.
64. Love MI, Huber W, Anders S. Moderated estimation of fold change and dispersion for RNA-seq data with DESeq2. Genome Biol. 2014;15:550.
65. Stephens M. False discovery rates: a new deal. Biostatistics 2016;18:275–94.
66. Xie J, Mao Q, Tai PWL, He R, Ai J, Su Q, et al. Short DNA hairpins compromise recombinant adeno-associated virus genome homogeneity. Mol Ther. 2017;25:1363–74.

ACKNOWLEDGEMENTS

We would like to thank Drs. Paola Divieti Pajevic and Marc Wein for providing Ocy454 osteocytic cell line. We also thank the many individuals who provided valuable reagents. This research was supported by Basic Science Research Program through the National Research Foundation of Korea (NRF) funded by the Ministry of Education (2014R1A6A3A03055719, J.M.K.). This project was also supported by the Center for Skeletal Research Imaging and Biomechanical Testing Core for biomechanical testing (NIH P30AR066261) and Career Award for Medical Scientists from the Burroughs Wellcome Fund, the NIH under awards DP5OD021351 and R01AR075585, and a Pershing Square Sohn Cancer Research Alliance award to M.B.G. J.H.S holds support from NIAMS of the NIH under R01AR068983 and R21AR077557 and the AAVAA Therapeutics.

AUTHOR CONTRIBUTIONS

J.M.K. designed, executed, and interpreted the experiments. Y.Y.S, J.K., and O.L. performed histology, immunohistochemistry, dynamic histomorphometry, and micro-CT analyses. J.X., and G.G. generated rAAV. J.H., and H.C. performed transcriptome analysis. B.B., and O.F. generated and provided Csnk2b floxed mice, respectively. M.B.G. helped skeletal analysis of mice. J.H.S. supervised the research and participated in the manuscript preparation.

COMPETING INTERESTS

JHS is a scientific co-founder of the AAVAA Therapeutics and holds equity in this company. GG is a scientific co-founder of AAVAA Therapeutics, Voyager Therapeutics, and Aspa Therapeutics and holds equity in these companies. GG is an inventor on patents with potential royalties licensed to Voyager Therapeutics, Aspa Therapeutics Inc., and other biopharmaceutical companies. Other authors declare no competing interests.

ETHICS APPROVAL

All animals were used in accordance with the NIH Guide for the Care and Use of Laboratory Animals and were handled according to protocols approved by the University of Massachusetts Medical School on animal care (IACUC).

ADDITIONAL INFORMATION

Supplementary information The online version contains supplementary material available at https://doi.org/10.1038/s41418-022-00952-x.

Correspondence and requests for materials should be addressed to Jae-Hyuck Shim.

Reprints and permission information is available at http://www.nature.com/reprints

Publisher's note Springer Nature remains neutral with regard to jurisdictional claims in published maps and institutional affiliations.